Overview of interpretive modelling of fusion performance in JET DTE2 discharges with TRANSP

Ž. Štancar[a,*], K. Kirov[a], F. Auriemma[b], H.-T. Kim[a], M. Poradziński[a], R. Sharma[a], R. Lorenzini[b], Z. Ghani[a], M. Gorelenkova[c], F. Poli[c], A. Boboc[a], S. Brezinsek[d], P. Carvalho[a], F. J. Casson[a], C. Challis[a], E. Delabie[a], D. Van Eester[e], M. Fitzgerald[a], J. M. Fontdecaba[f], J. Garcia[g], L. Garzotti[a], C. Giroud[a], A. Kappatou[h], Y. Kazakov[e], D. King[a], V. Kiptily[a], D. Kos[a], E. Lerche[e], E. Litherland-Smith[a], C. Maggi[a], P. Mantica[i], M. J. Mantsinen[j], M. Maslov[a], S. Menmuir[a], M. Nocente[l], J. Oliver[a], S. Sharapov[a], P. Sirén[a], E. R. Solano[f], H. J. Sun[a], G. Szepesi[a], JET Contributors[k]

[a] *United Kingdom Atomic Energy Authority, Culham Science Centre, Abingdon, UK*
[b] *Consorzio RFX, ISTP-CNR, Padova, Italy*
[c] *Princeton Plasma Physics Laboratory, Princeton, USA*
[d] *Forschungszentrum Jülich, Insitut für Energie und Klimaforschung–Plasmasphysik, Jülich, Germany*
[e] *Laboratory for Plasma Physics, Ecole Royale Militaire, Brussels, Belgium*
[f] *Laboratorio Nacional de Fusión, CIEMAT, Madrid, Spain*
[g] *CEA, Cadarache, France*
[h] *Max-Planck-Institut für Plasmaphysik, Garching, German*
[i] *ISTP-CNR, Milano, Italy*
[j] *Barcelona Supercomputing Center, Barcelona, Spain*
[k] *Dipartimento di Fisica "G. Occhialini", Università di Milano-Bicocca, Milan, Italy*
[l] *See the author list of 'Overview of JET results for optimising ITER operation' by J. Mailloux et al 2022 Nucl. Fusion 62 042026*

Abstract

In the paper we present an overview of interpretive modelling of a database of JET-ILW 2021 D-T discharges using the TRANSP code. Our main aim is to assess our capability of computationally reproducing the fusion performance of various D-T plasma scenarios using different external heating and D-T mixtures, and understand the performance driving mechanisms. We find that interpretive simulations confirm a general exponential relationship between increasing external heating power and fusion output, which is supported by absolutely calibrated neutron yield measurements. Comparing measured and computed D-T neutron rates we find a strong dependency of the discrepancy between the two and absolute neutron rate. The calculations are found to agree well with measurements for higher performing discharges with external heating power above $\sim$ 20 MW, while low-neutron shots display an average discrepancy of around + 40 %. A similar trend is found for the ratio between thermal and beam-target fusion, where larger discrepancies are in average seen in shots with beam-driven performance. We compare the observations to studies of JET-ILW D discharges, to find that in average the fusion performance is well modelled over a range of heating power, although an increased unsystematic deviation for lower-performing shots is observed. The ratio between beam-induced and thermal D-T ion fusion is found to be increasing with a weak exponential dependency, with the maximum achieved value of $\gtrsim 1$ in a baseline experiment. An assessment of the fusion power computational uncertainty due to uncertainty in the input data shows a strong dependency on the plasma scenario due to the sensitivity to performance drive mechanisms, varying between ± 25 – 35 %. Alpha particle simulations have shown that the ratio between volume-integrated electron and ion heating from alphas is $\lesssim 10$ for the majority of discharges, with alpha electron heating power reaching a maximum of $\sim$ 70 % with respect to that provided by combined beam and RF injection in the core. An alternative

workflow was needed to correctly model the DTE2 shots with highest fusion yield because of the use of fundamental majority RF heating, which was calculated to have provided ~ 10 % to the total fusion power.

Keywords:
Deuterium-tritium plasma, Integrated modelling, Fusion performance, JET, TRANSP

1. Introduction

Fusion power measurements are an essential tokamak operational parameter from the perspective of safety as well as tracking progress towards achieving burning plasma conditions. It is therefore important to develop and validate integrated modelling tools capable of interpreting the fusion performance of current experiments, and making accurate predictions in ITER-like conditions and those expected in pilot fusion plants. A range of plasma scenarios with varying fusion performance was tested in JET's 2021 deuterium-tritium campaign (DTE2) with the ITER-like-wall (ILW, metal Be/W), which provided a unique opportunity to benchmark interpretive plasma modelling codes.

In the paper we present an overview of interpretive modelling of over 80 JET ILW DTE2 discharges using the TRANSP code [1, 2, 3]. The main aim is to analyse our capability of reproducing the fusion performance of various D-T plasma scenarios, in which different external heating and D-T mixture configurations were used in an effort to maximize the fusion energy output. We summarize the main motivation for this work in the following points:

(i) JET has the unique capability to measure time-dependent absolute fusion power produced in D-T plasmas due to its absolutely calibrated 14 MeV neutron detectors [4, 5]. In the calibration procedure a D-T neutron generator is moved through the vacuum vessel with the help of a remote handling system in a series of toroidal and poloidal positions. In the process the response and spatial sensitivity of three independent fission chambers and the neutron activation system to a 14 MeV neutron source is measured. It is the neutron activation system that is absolutely validated in the calibration procedure due to its proximity to the plasma source, while the fission chambers are cross-calibrated against it. The complex procedure, which requires detailed neutron transport calculational support and dedicated plasma calibration discharges, has a total uncertainty below ~ 10 % and is planned to be applied to ITER [6, 7, 8, 9]. In this work we exploit the absolute neutron yield measurements obtained in DTE2 to benchmark state-of-the-art plasma code calculations, and provide a foundation to validate and tune predictive models. This enables the development of multi-physics whole-device workflows and synthetic diagnostics models, facilitating reliable fusion performance extrapolations for ITER and future fusion devices [10, 11].

(ii) Previous interpretive modelling work aimed at reproducing JET's fusion performance in D and D-T plasmas achieved various degrees of agreement between calculations and measurements. Most notably a general over-prediction of the computed neutron yield was observed over a range of studies with codes such as TRANSP and ASCOT [12, 13, 14, 15, 16, 17, 18]. A comprehensive analysis of JET D plasma performance with a carbon wall is presented in [12], where it is found that the calculations overestimate the measured neutron rates by up to 50 %, independently of fusion performance or its drivers. The cause of the observed "neutron deficit" is investigated through uncertainties in fuel

*Corresponding author
Email address: ziga.stancar@ukaea.uk (Ž. Štancar)

dilution, equilibrium mapping errors, NBI power and penetration, as well as broadband and MHD transport. No single mechanism was found to explain the observations, while it was postulated that an unfavourable combination of systematic modelling errors might play a role. The study published in [13] looks at JET's trace tritium experiments in which a T beam was injected into a pure D plasma. Similarly, the study had observed an overestimation of the computed fusion power for both the D-D and D-T neutron dominated phases, which was pronounced in higher density plasmas. In order to obtain a match in the neutron rates the authors artificially applied a reduction in T-NBI power of up to 40 % and a fast ion anomalous diffusion between 5 and 10 m^2/s. These are large values both for the expected uncertainty in beam power, as well as observed anomalous transport. Additionally no effect of the growth of low n/m MHD modes on the neutron yield was found. The remaining studies listed above focus on analysing the neutron yield in JET-ILW D or DTE1 experiments, and observe an improvement in computational agreement for higher performing discharges. In summary, an unambiguous explanation for the discrepancies between measured and computed fusion power has not been identified in preceding work, with suspected contributing causes varying from systematic experimental uncertainties in input data to unaccounted fast ion turbulent transport. In this paper we revisit the fusion power comparison through a large database of JET-ILW D and D-T plasma TRANSP runs. The discharges' plasma parameters cover a wide range of plasma current, B-field, electron density, electron and ion temperature, external heating power, etc. values – resulting in variations of neutron yields over several orders of magnitude. Additionally an improved modelling workflow has been adopted, which facilitates modelling consistency and evaluation of systematic input uncertainty.

(iii) An important physics outcome of JET's DTE2 experiment is the insight into alpha particle physics, e.g. to understand the role alphas play in plasma self-heating, and driving plasma instabilities such as Alfvén eigenmodes. Because the alpha particle source is linearly proportional to the neutron yield, the fidelity of alpha particle effects modelling is related to our capability to reproduce the fusion performance. In the paper we present an overview of the calculated trends of alpha power flow into the electron and ion channels, and assess the alpha pressure and power in comparison with the fast NBI ions.

(iv) Probing the readiness of interpretive capabilities of TRANSP for analyses of D-T fusion performance, we find that the best performing pulses in the DTE2 campaign, the hybrid-like T-rich scenario highly driven by beam-target fusion, cannot be modelled fully with default TRANSP capabilities. Namely in the scenario the fundamental D majority RF heating is applied – while the evolution of the resulting fast deuteron ions can be performed in TRANSP with the FPP code, this is not communicated to the fusion reactivity calculator – adopting an alternative modelling workflow, we assess the additional contribution to the total fusion output.

(v) New deuterium-tritium plasma results have been produced in JET's DTE2 campaign more than 20 years after DTE1 [19]. In this time significant progress has been made in the understanding of tokamak physics, development of plasma modelling workflows, and improvement of JET's diagnostics systems [20, 21]. Throughout the paper we showcase the effect of these joint improvements on integrated modelling, discuss advancements in diagnostics analysis and code fidelity, and address the modelling challenges encountered.

The paper is structured as follows: in *Section 2* the modelling workflow is presented, emphasizing the importance of consistent preparation of input data and equilibrium reconstruction. We describe the modelling tools used, detail which diagnostics are used for the preparation of input and their fits, and showcase how these are validated. We describe the JET-ILW DTE2 and D campaign discharge databases, followed by a display of the regular consistency checks for the DTE2 dataset, i.e. agreement between measurements and

synthetic TRANSP signals for integrated electron density, plasma stored energy, neutron yield, and D-T fuel mixture. In *Section 3* we delve deeper into the analysis of fusion power calculations, which is split into several sub-sections: *Section 3.1* describes fusion reactivity drivers for a selection of plasma scenarios, which we tie to the relationship between thermal and beam-target fusion contributions. We elaborate on the role of NBI and RF heating, and the effects these have on the electron and ion power balance, in addition to beam density peaking in D-T, T_i/T_e and rotation, and effective collisionality. We discuss the excellent match between DTE2 measurements and simulations for high performance discharges, and the over-prediction observed for lower-performing ones. We compare the findings to the results from JET-ILW D campaigns, and discuss potential reasons for the observed discrepancies; *Section 3.2* delves into uncertainties of D-T relevant quantities – we chose three discharges from the low- and high-power branch (NBI-only neutron calibration discharge #99812, baseline #99863, and hybrid #99950) and vary parameters like the D-T fuel ratio, n_e, T_e, T_i, within their respective uncertainties and produce a computational uncertainty assessment; *Section 3.3* discusses the observation from fusion alpha modelling, focusing on the trends of alpha heating of electrons and ions, as well as the alpha pressure. In *Section 4* we describe the modelling challenges we have encountered in DTE2 with TRANSP and its heating modules. We will study one of the T-rich record shots #99972, in which the fundamental RF heating of a thermal D population is expected to contribute up to $\sim$ 15 % to the total neutron rate, which is not computed in TRANSP by default. We will showcase how we evolve the D-RF tail with a Fokker-Planck solver and use this distribution function to calculate the additional D-T fusion rate. In *Section 5*, the discussion and conclusions section, the highlight findings of the project are presented, together with a description of future work and modelling suggestions, especially from the perspective of improving the fusion power match for low-power discharges. We comment on how the reference interpretive runs will be used in further studies.

2. Integrated modelling workflow

2.1. TRANSP database

The results presented in the following chapters are based on data obtained during the JET-ILW D (*C38* in 2016-2020) and DTE2 (*C41* in 2021) campaigns. The database of interpretive runs comprises 79 deuterium discharges (with some discharges including a ^{1}H or ^{3}He second thermal species with concentrations larger than that of a typical RF minority, i.e. $\gtrsim$ 5 %) and 87 deuterium-tritium discharges (with varying ratios of D-T fuel mixture). Both databases include a variety of plasma scenarios – from the perspective of fusion performance the scenarios exhibit large variations in fusion power and differ in the mechanisms driving the performance. The criteria for selecting which discharges to model were mainly the availability of validated diagnostics data and the scientific relevancy of the experiment. Generally it is the higher performing discharges that have been designed and optimized to sustain and maximize fusion power, while the lower performing shots are aimed at triggering specific plasma physics phenomena with little need for high fusion output. In the analysis we exploit the broad range of shot characteristics to identify fusion performance and computational fidelity trends. Throughout the paper we adopt a discharge notation based on the scenario type, described in detail in the bullets below. The discharge types that are not directly addressed in the paper are labelled as *"other"*, and were predominantly performed at lower density, current, and heating power with varying D-T composition:

- *Baseline*: ELMy H-mode scenario generally performed at high toroidal current $I_p \geq 3.0$ MA, toroidal field $B_t \sim 3.3$ T, safety factor of $q_0 < 1$ and $q_{95} \sim 3$, beta values of $\beta_P < 1$ and $\beta_N \sim 1.8$–2.0, high electron density, mixed D-T NBI and H RF minority heating, aiming at maximizing thermal fusion performance [20, 22, 23];

- *Hybrid*: ELMy H-mode scenario generally performed at lower current than baseline with $2.2 \leq I_p \leq 2.5$ MA, toroidal field $B_t \sim 3.45$ T, shaped broad q-profile at $q_0 \geq 1$ and $4.5 \leq q_{95} \leq 5.0$, beta values of $\beta_P \geq 1$ and $\beta_N \sim 2.0$–2.3, modest electron density, mixed D-T NBI and H RF minority heating, aiming at improved stability and reduced core transport for better confinement [24, 25, 26];

- *T-rich*: hybrid-like scenario optimized to maximize non-thermal fusion with a D-T fuel mix of ∼ 15/85 %, single species D NBI and fundamental D RF heating – achieved fusion energy record in DTE2 [27, 28];

- *Energetic particle afterglow (EP)*: mixed D-T NBI-only heating with two reference plasmas – *ITB* lowest density discharges for high transient fusion power, exploiting q^2 scaling in TAE stability, performed at toroidal current $I_p = 2.9$ MA, toroidal field $B_t = 3.45$ T, elevated q-profile with $q_0 > 1.5$, $q_{95} = 3.8$ and conventional magnetic shear, with $\beta_N \sim 1.3$ and $T_i \gg 2T_e$. *Hybrid-like* scenario with highest transient fusion power, exploiting β_α scaling in TAE stability, performed at toroidal current $I_p = 2.3$ MA, toroidal field $B_t = 3.45$ T, with $\beta_N \sim 2$ [29, 30];

- *Radio-frequency (RF)*: mostly hybrid-like discharges at modest toroidal current $I_p \sim 2.5$ MA and varying toroidal field, employing different RF heating schemes, e.g. second harmonic D majority, second harmonic T majority, and ^{3}He minority [31, 32, 33, 34];

- *Seeded*: neon-seeded ELMy H-mode performed with $I_p = 2.5$ MA, toroidal field of $B_t = 2.8$ T, safety factor of $q_0 < 1$ and $q_{95} = 3.2$, beta values of $\beta_P < 1$ and $\beta_N \sim 1.2$–$2.$, high electron density, mixed D-T NBI and H RF minority heating, aiming at assessing core-edge integration of an ELMy H-mode in D-T with a partially detached divertor [35];

- *Calibration*: a lower-performing mixed D-T NBI-only discharge performed at a toroidal current of $I_p = 2.0$ MA and toroidal field of $B_t = 2.4$ T, aimed at cross-calibrating the neutron yield monitors against foil activation measurements by the neutron activation system. The calibration discharges were chosen as representatives of low-power shots, exhibiting similar operational parameters and fusion performance drivers.

All the discharges were modelled interpretively with TRANSP and its coupled heating modules – NUBEAM orbit tracking code for beam injected ions [36], and TORIC RF wave solver [37]. The integrated modelling framework OMFIT was used for orchestrating the input data preparation and analysis of the modelling results [38, 39]. The NBI + RF synergistic effects, important for example in discharges with 2nd harmonic RF acceleration of fast NBI ions, was modelled with the quasi-linear RF kick operator [40, 41]. The operator communicates the TORIC computed RF electric field components and perpendicular wave vector for each toroidal mode quantities to NUBEAM [42].

2.2. Input data preparation

In order for individual simulations to be comparable and enable a cross-scenario analysis, the input data preparation workflow was pre-defined, followed by data consistency checks. The interpretive analyses used fitted electron density and temperature profiles as input – fits for both quantities were done with high resolution Thomson scattering (HRTS) data [43], with the temperature additionally constrained by electron cyclotron emission data [44]. Thomson scattering n_e measurements are cross-calibrated against the absolutely calibrated interferometer line-integrated density. Because this is done in discharges' ohmic phase a discrepancy between HRTS and interferometer measurements can be observed in the heating phase, which

has been found to increase proportionally to T_e. The discrepancy is corrected by applying a radially independent scalar scaling to HRTS data, in average varying between $1.0 \sim 0.9$, with the correction factor generally larger with increasing external heating power. The ion temperature and rotation were prescribed based on fits from core and edge charge-exchange (CX) diagnostics – while these measurements were generally of good quality with the carbon wall, the inherent CX conditions are less favourable in the Be/W wall, often resulting in poor T_i data [45, 46]. Neon puffing is commonly used to enhance the CX signal strength, but measurements in the core are still strongly affected by the diffusion of Ne gas from the edge, which is dependent on the plasma density. It is therefore not uncommon for the quality of the CX signal to be poor close to the magnetic axis, i.e. $\rho \lesssim 0.3$, which can strongly affect the calculation of the total fusion rate. To better constrain T_i and plasma rotation fits in the core, additional surrogate points can be obtained through electron-ion equipartition and power balance calculations [47].

The equilibrium and safety factor were taken from an EFIT++ time-evolved reconstruction constrained by an improved magnetics measurements suite and realistic pressure profiles, i.e. including kinetic profile fits and NBI/RF accelerated fast ions, as well as MHD markers and polarimetry measurements [48]. The equilibrium was applied to kinetic profile data mapping and was fully prescribed in TRANSP, i.e. an internal solver was not used. In order to obtain a converged equilibrium solution an iterative approach was adopted, starting with a magnetics-only reconstruction, which was fed into TRANSP to obtain an improved plasma pressure profile. This was followed by consecutive steps including mapping, executing TRANSP, and EFIT++ reconstructions, until a close match was reached with the preceding iteration (two iterations were generally sufficient). Through this improved equilibrium reconstruction method we observed a consistent match between the equilibrium-computed boundary location and the one inferred by density and temperature edge measurements, as well as agreement between the EFIT++ and TRANSP calculated plasma stored energy. In contrast the use of more rudimentary EFIT reconstruction methods resulted in the need to radially shift density and temperature profiles to obtain reasonable separatrix values, and led to a systematic mismatch in the stored energy calculated in the reconstruction and modelling codes. An example of an embedded fit consistency check for the baseline discharge #99863 is shown in Figure 1, where the electron density, electron temperature, ion temperature and toroidal rotation fits are compared against diagnostics measurements described above. In panel *(c)* of Figure 1 one can observe that the T_i CX measurements closes to the axis, at $\rho \sim 0.25$, have values below the expected fit trend – this is due to the low CX signal intensity discussed above, albeit there was Ne injected. A T_i surrogate estimate derived from power balance constraints, depicted with a red circle symbol, was used as an additional core constraint. The CX measurements are divided into four diagnostics groups with two denoting core measurements (magenta and yellow), and two edge measurements (green and blue). If available CX data with cross section and fine-structure corrections was used [49].

The deuterium-tritium plasma composition was prescribed based on measurements of relative H+D+T hydrogenic species concentrations by the residual gas analysis diagnostics, located in the divertor pump [50]. Since this is an edge measurement the D-T fuel mixture has to be extrapolated to the core, which was done by including impurity and beam dilution corrections. The beam dilution correction requires an iterative approach because it is based on a beam density calculation stemming from a converged slowing-down solution. This means that the core D-T ratio in the first run is computed using a prescribed surrogate beam dilution profile with a beam concentration estimate of ~ 5 % with respect to n_e. In the following simulation's D-T composition extrapolation, the NUBEAM computed beam density profile is available (two iterations were generally sufficient). It was found that the computed core value of D/T concentration coincided closely with the edge value, which is addressed in more detail in 3.2. The fuel mix concentrations were cross-checked against an independent measurement by divertor optical gas spectroscopy [51]. The

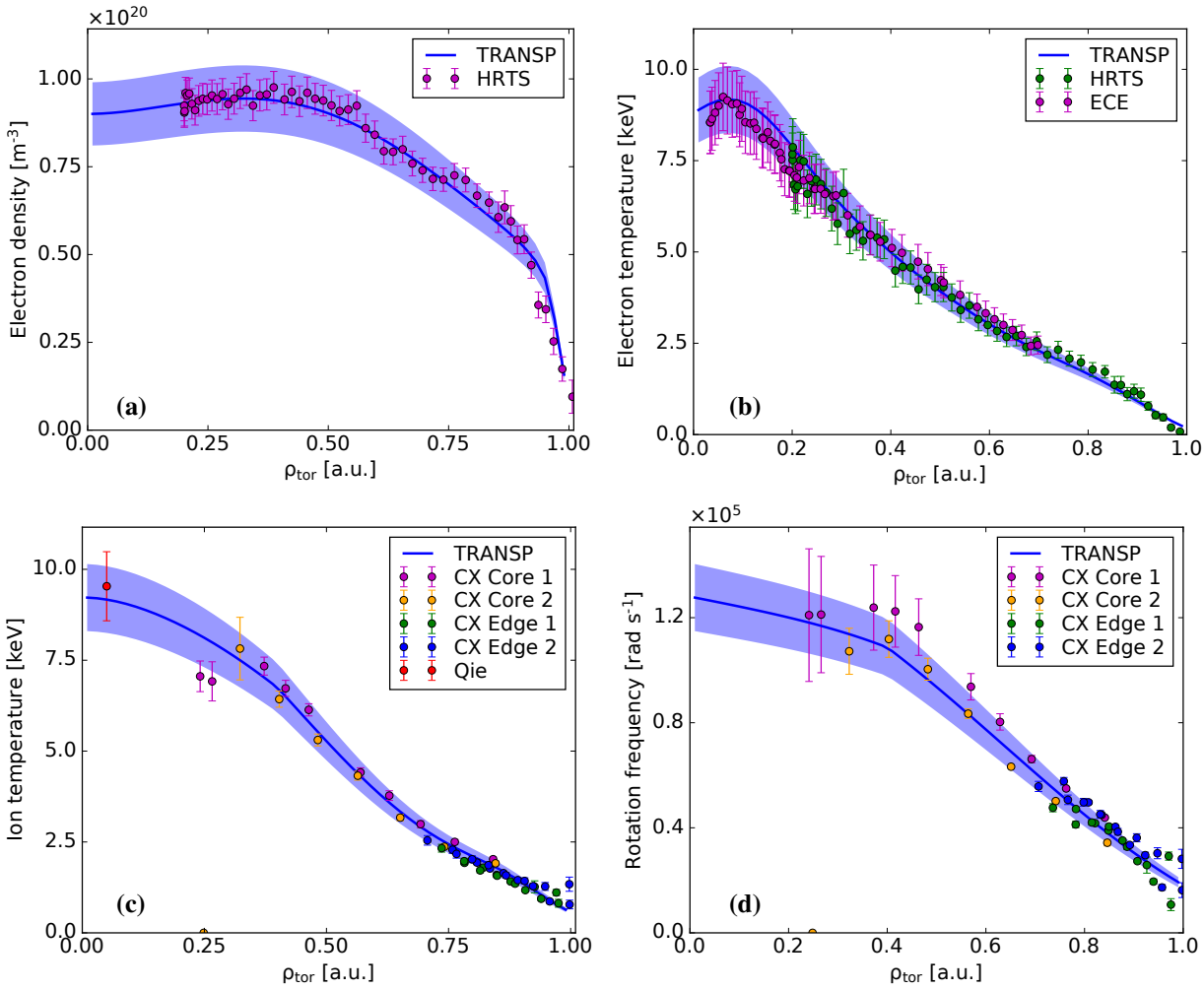

Figure 1: Example of a comparison between measurements (circles) and fits (solid blue with 10 % uncertainty) used as input in TRANSP interpretive simulations for baseline discharge #99863 at 49.55 s – *(a)*: electron density with HRTS measurements, *(b)*: electron temperature with HRTS measurements, *(c)*: ion temperature with CX measurements and ion-electron equipartition surrogate calculation (red), *(d)*: toroidal rotation with CX measurements. The x-axis is TRANSP's native ρ_{tor} radial coordinate – root of the normalized toroidal magnetic flux $\sqrt{\Psi_{tn}}$. The blue shaded areas denote a 10 % fit uncertainty.

concentration of the RF minority was prescribed based on residual gas analysis as a fixed fraction of the electron density, with an average value between 2.5 % - 5.0 %, with protium being the most common RF species and individual discharges employing ^{3}He. Through a combined analysis of the effective charge, soft X-ray, bolometry, and charge-exchange-recombination spectroscopy measurements it is possible to obtain a good estimate of the impurity composition at JET [52], however such analyses are time-consuming and were not yet available for the majority of the database discharges. In order to unify the prescribed impurity composition across the database, we assumed a generic metallic wall mixture. That is a fixed value of 1 % Be and 0.02–0.05 % Ni, stemming from average CX analyses values, with the remainder ascribed to W or Ne (depending on presence of puffing/seeding) based on a quasi-neutrality calculation constrained by visible spectroscopy ZEFF measurements, assuming a flat profile. While ZEFF, radiation, and impurity density are expected to exhibit profile shapes governed by inward neoclassical transport and rotation [53, 54], the

low-Z impurities largely responsible for dilution can be approximated with a scaled electron density profile reasonably well. There was no additional anomalous transport imposed and no sawtooth model was applied. The interpretive simulations were performed with time-resolved kinetic profiles and external heating, while the presented database results are averaged over a one second interval in the steady-state highest-performing part of the discharges.

2.3. Consistency checks

The quality of TRANSP results is largely dependent on the effort invested into rigorously preparing the input magnetic equilibria and profiles, and ensuring basic output plasma parameters match the standard consistency measurements. The three basic global parameter consistency checks that are performed after every TRANSP analysis to ensure the quality of a given run are the line-integrated electron density, diamagnetic energy and neutron rates. It is worth noting that these three parameters represent the minimum required set, while more checks potentially need to be made, depending on the scenario type and physics aim. The TRANSP output contains a synthetic line-integrated electron density interferometer signal, which models the response seen by JET's laser interferometer channels [55]. A direct comparison to the measured interferometer data enables a check of the HRTS measured density profiles, which are cross-calibrated against the interferometer, and supports the density fits, as well as the quality of the magnetic equilibrium reconstruction. Generally the interferometer line-of-sight measuring the electron density closest to the plasma core is used. The diamagnetic energy is calculated as part of the equilibrium reconstruction with EFIT++ and includes the plasma diamagnetic energy and the plasma MHD energy. These quantities are not output by TRANSP by default and are derived from the the thermal W_{th}, and fast ion parallel $W_{f\parallel}$ and perpendicular $W_{f\perp}$ energy components as $W_{\mathrm{dia}} = W_{\mathrm{th}} + 1.5\ W_{f\perp}$ and $W_{\mathrm{MHD}} = W_{\mathrm{th}} + 1.5\ (W_{f\parallel} + 0.5\ W_{f\perp})$. In D-T plasmas the total neutron yield Y_n is directly proportional to the fusion energy produced, i.e. $E_{\mathrm{D-T}} = Y_{\mathrm{n}}(\langle E_{\mathrm{n}}\rangle + \langle E_{\alpha}\rangle)$, where $\langle E_{\mathrm{n}}\rangle$ and $\langle E_{\alpha}\rangle$ are the average energies of D-T fusion neutrons at ~ 14.1 MeV and alphas at ~ 3.5 MeV. At JET the neutron yield is measured by absolutely calibrated fission chambers [4, 5]. The total yield is obtained as the time integral of the measured neutron rate R_n, which is defined as:

$$R_{\mathrm{n}} = \int_V \frac{1}{1+\delta_{\mathrm{ab}}} n_{\mathrm{a}} n_{\mathrm{b}} \langle \sigma v \rangle \, dV \,, \tag{1}$$

i.e. a volume integral of the number of fusion reactions per unit time and unit volume, between two ion species with densities n_{a} and n_{b}, where δ_{ab} is the Kronecker delta, included to avoid the double counting of reactions when two ions of the same species are considered. The fusion reactivity $\langle \sigma v \rangle$ is defined as the integral over the ion velocity distribution functions f_{a} and f_{b} and the cross section for the reaction σ_{ab}:

$$\langle \sigma v \rangle = \int_{\mathbf{v}_{\mathrm{a}}} \int_{\mathbf{v}_{\mathrm{b}}} f_{\mathrm{a}}(\mathbf{v}_{\mathrm{a}}) f_{\mathrm{b}}(\mathbf{v}_{\mathrm{b}}) \mathbf{v}_{\mathrm{rel}} \sigma_{ab}(\mathbf{v}_{\mathrm{rel}}) d\mathbf{v}_{\mathrm{a}} d\mathbf{v}_{\mathrm{b}} \,, \tag{2}$$

where $\mathbf{v}_{\mathrm{a}}$ and $\mathbf{v}_{\mathrm{b}}$ are the velocity vectors of the interacting ions and $\mathbf{v}_{\mathrm{rel}}$ their relative velocity. Fusion reactivity can be computed by either semi-analytical or numerical integration techniques [56, 57, 58]. The total neutron emission in D-T plasmas with a mixed fuel and beam ion composition comprises neutrons originating from various combinations of fusion interaction between different isotopes and ion populations – most commonly these are divided into thermal ion interactions (*TH*), fast-thermal ion interactions (commonly labelled beam-target, *BT*), and fast-fast ion interactions (commonly labelled beam-beam, *BB*). The total neutron rate from Equation 1 can be expanded into:

$$R_{\mathrm{n}}\,(DT) = \int_V \Big(n_{\mathrm{d}} n_{\mathrm{t}} \langle \sigma v \rangle_{\mathrm{TH}}(DT) + n_{\mathrm{db}} n_{\mathrm{t}} \langle \sigma v \rangle_{\mathrm{BT}}(D \rightarrow T) + n_{\mathrm{d}} n_{\mathrm{tb}} \langle \sigma v \rangle_{\mathrm{BT}}(T \rightarrow D) + n_{\mathrm{db}} n_{\mathrm{tb}} \langle \sigma v \rangle_{\mathrm{BB}}(DT) \; + \\ + \; \frac{1}{2} n_{\mathrm{d}} n_{\mathrm{d}} \langle \sigma v \rangle_{\mathrm{TH}}(DD) + n_{\mathrm{d}} n_{\mathrm{db}} \langle \sigma v \rangle_{\mathrm{BT}}(D \rightarrow D) + \frac{1}{2} n_{\mathrm{db}} n_{\mathrm{db}} \langle \sigma v \rangle_{\mathrm{BB}}(DD) + \\ + \; n_{\mathrm{t}} n_{\mathrm{t}} \langle \sigma v \rangle_{\mathrm{TH}}(TT) + 2 n_{\mathrm{t}} n_{\mathrm{tb}} \langle \sigma v \rangle_{\mathrm{BT}}(T \rightarrow T) + n_{\mathrm{tb}} n_{\mathrm{tb}} \langle \sigma v \rangle_{\mathrm{BB}}(TT) \Big) \, dV \; , \tag{3}$$

comprising D-T, D-D and T-T neutron contributions. The thermal fuel ion densities are denoted n_{d} and n_{t}, while for the beam population densities n_{db} and n_{tb} are used. TRANSP calculates the total rate of neutron emission as well as its source components – thermal, beam-target and beam-beam fusion. In the paper we compare the calculated values against the total neutron rate measured by fission chambers. In addition to the three standard consistency checks, we also confirm that the measurements of the edge D-T fuel mix concentrations are preserved when prescribing the initial plasma composition in TRANSP. Therefore the divertor residual gas measurements of $n_{\mathrm{d}}/(n_{\mathrm{d}} + n_{\mathrm{t}})$ are compared to the TRANSP ion density output at the edge.

Figure 2 shows the measurements vs. calculation consistency plots for the global parameters of the DTE2 discharge database, in which we adopt a symbol notation corresponding to the scenario description at the beginning of Section 2. The black dashed lines denote equality between the measurements and calculations, while the green dashed lines denote the combined experimental and computational uncertainty, evaluated to be around ± 10 % for n_{e}, W_{dia}, and $n_{\mathrm{d}}/(n_{\mathrm{d}} + n_{\mathrm{t}})$, and ± 25 % for the neutron yield. Both the line-integrated density and diamagnetic energy calculations in panels *(a)* and *(b)* align well with the measurements within the uncertainty, while showing signs of grouping according to the characteristics of the individual scenario. It can be seen that the baseline experiments were performed at some of the highest densities achieved in D-T, in combination with the highest diamagnetic energy of ∼ 10 MJ. Both the hybrid and T-rich scenarios were performed at mid-range density with diamagnetic energy clustered at around 8 MJ. The neutron yield comparison in panel *(c)* shows a more heterogeneous picture. One can observe that the bulk of the high performance pulse calculations, with neutron rates between $1{\cdot}10^{18}$ – $4{\cdot}10^{18}$ s^{-1}, agrees with the measurements well. These mostly include plasma scenarios in which the fusion power output was optimized throughout the campaign, e.g. baseline, hybrid, RF, and EP. On the other hand the lowest performing discharges with rates below $1{\cdot}10^{18}$ s^{-1} overestimate the measurements, as do the best performing, record T-rich pulses of DTE2. These produced neutrons at rates just above $4{\cdot}10^{18}$ s^{-1}, with calculations up to 25 % higher than the measurements, but still within the estimated uncertainty. The additional edge fuel mix check presented in panel *(d)* shows that the edge fuel ion densities are prescribed and evolved in TRANSP in accordance with the measurement constraint. To summarize – a general observation for the four consistency checks is that a relatively good and satisfactory match between the measured and computed values is achieved, within the estimated uncertainty, which forms a reliable basis for the conclusions we draw in the following sections.

3. Fusion performance analysis

In this section we present results obtained through a comparative analysis of the DTE2 discharge database. We focus on three major topics: *(i)* understanding the fusion performance drivers of various scenario types and trends of fusion output optimization, and the overall performance of the interpretive

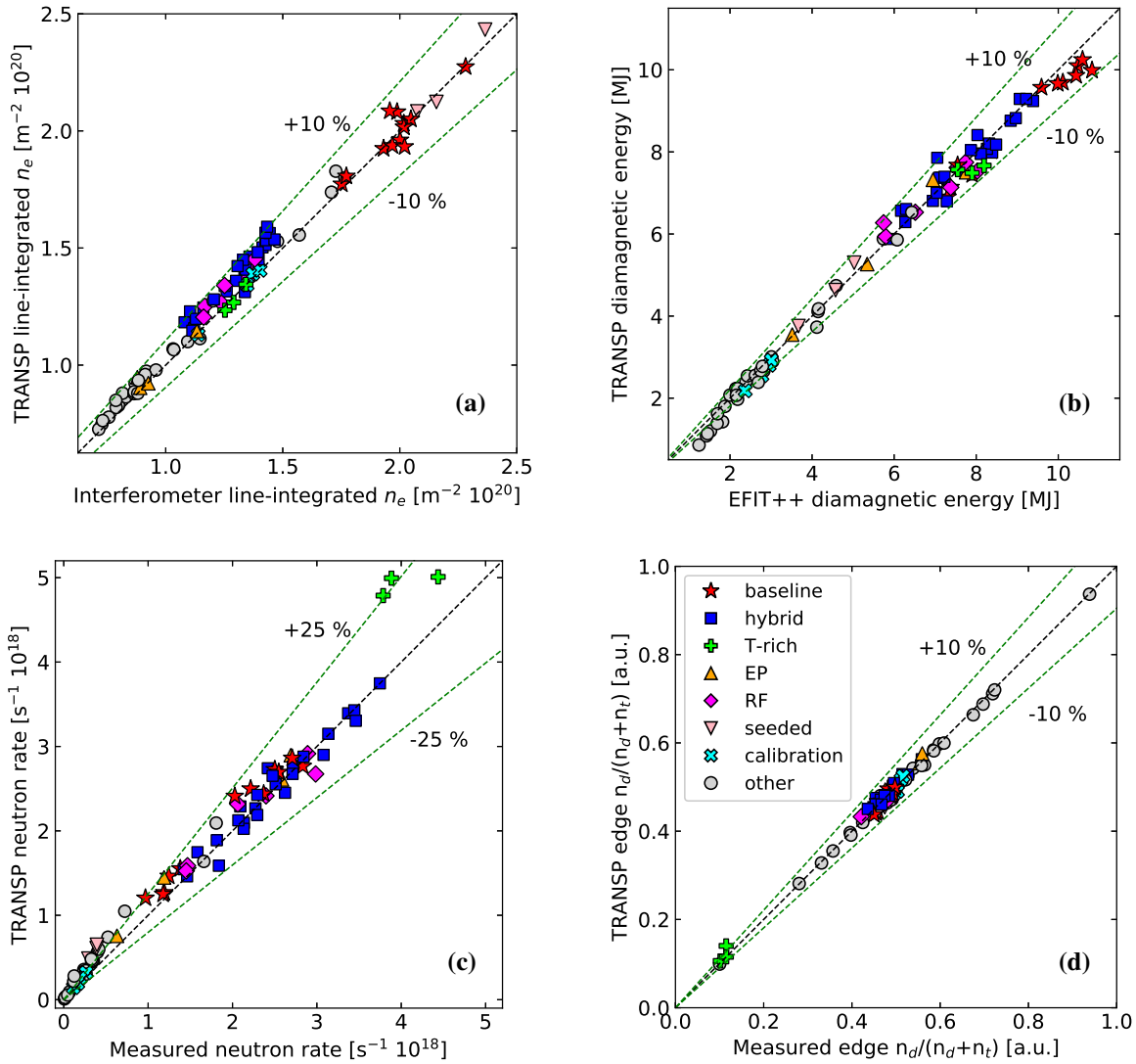

Figure 2: Consistency checks between measurements (x-axis) and TRANSP interpretive calculations (y-axis, 1 s average) for the DTE2 database – *(a)*: core line-integrated electron density interferometer measurements and TRANSP synthetic diagnostic, *(b)*: plasma diamagnetic energy W_{dia} computed by EFIT++ and TRANSP, *(c)*: neutron rate fission chamber measurements and TRANSP calculations, *(d)*: divertor residual gas measurements of the edge $n_d/(n_d + n_t)$ fuel mix and equivalent TRANSP calculations. The grey dotted lines denote the combined experimental and computational uncertainty band. The graphs share the scenario type legend notation.

fusion power calculations against absolutely calibrated measurements; *(ii)* assessing the fusion power computational uncertainty and its dependency on scenario type; *(iii)* overview of fusion alpha performance in the D-T experiments and the potential trends for future experiments.

3.1. Performance drivers

One of the goals of JET's DTE2 campaign was to maximise the fusion power output compared to the preceding DTE1 achievements in a sustained way [19, 59]. Based on results from deuterium campaigns

with the ITER-like-wall, two stationary plasma scenarios with the potential of delivering the objective were identified - the baseline and hybrid discharges. Modelling work was done to assess the level of expected fusion power output based on the best performing deuterium discharges. This was done with two methods – rudimentary D-T equivalent fusion power calculations, in which it was assumed that the plasma kinetic profiles are the same as in D with the fuel mix altered to 50:50 D-T, and through advanced first-principles based predictive modelling, in which the kinetic profiles are evolved taking into account phenomena like the isotope effect, through energy exchange or $E \times B$ shear stabilization, and fusion alpha heating [59, 20, 10]. Both methods agreed in predicting the extrapolated fusion output to reach levels between 9 ~ 15 MW with uncertainties of up to ± 2 MW, at an assumed total external heating power of 40 MW. It was observed that the predictive extrapolations of the fusion power displayed a strong power function relationship with the external plasma heating.

The high fusion performance branch of DTE2 experiments has confirmed these observations, albeit with the combined NBI and RF power reaching maximum values of around 35 MW, falling short of the extrapolation assumptions. In Figure 3 we display how the one-second-averaged TRANSP computed power depends on the total external heating power P_{heat} for the DTE2 modelling database. A clear power-law dependency can be seen between the two quantities, with the fusion power gain rate increasing with added heating power. One can observe that the scenarios show signs of branching – the baseline scenario's best-performing discharges are clustered at around 8 MW and are located on the lower part of the power curve, meaning that more heating power is required to match the output of other high-performance scenarios. One can observe that the hybrid power branch average is approximately 20 % higher compared to the baseline for the same input power, reaching a maximum fusion power output of ~ 10 MW. The highest-performing discharges of the campaign were the hybrid-like T-rich plasmas, in which the fuel mixture and beam settings were adjusted to maximize fusion reactivity. This was achieved by setting the beam species to deuterium-only, and the thermal ion species being predominantly tritium, in order to exploit the favourable fast deuterium → thermal T reactivity at beam injection energy of ~ 110 keV [60]. The scenario produced a discharge with the largest fusion energy output ever at 59 MJ integrated over the whole discharge. Two of the modelled EP scenario discharges, employing a hybrid-like scheme using only NBI heating, produced the highest fusion power output and central T_i per MW of external heating. In Figure 3 the two EP-hybrid discharges are located in the upper part of the discharge cluster, indicating a high fusion power rise rate. The EP discharges also achieved some of the highest transient fusion powers of 11-12 MW. The seeded experiments have achieved the lowest fusion performance per P_{heat}. The z-axis represents the fusion gain factor Q_{DT} defined as $P_{\mathrm{fus}}/P_{\mathrm{heat}}$, which is seen to steadily rise with increasing performance. The calculated max one-second-average sustained Q_{DT} for the baseline, hybrid and T-rich scenarios are 0.26, 0.32 and 0.41, respectively. One of the highest transient Q_{DT} values of ~ 0.45 was achieved by the EP-hybrid scenario. For comparison we plot a selection of TRANSP calculations for stationary baseline discharges from the DTE1 campaign (cyan stars) [14]. One can see that while the $P_{\mathrm{fus}}/P_{\mathrm{heat}}$ trend is similar to the bulk of the DTE2 cluster, the performance of the JET-C baseline discharges is better compared to the recent JET-ILW results of the same scenario. The best performing DTE1 steady-state baseline discharge #42982 achieved a fusion power output of ~ 4.6 MW and $Q_{\mathrm{DT}} = 0.19$ (encircled).

In Figure 4 the computed radial profiles of the local fusion gain factor q_{DT} are shown. It is computed as the ratio between the profiles of plasma heating and fusion power power densities $p_{\mathrm{heat}}/p_{\mathrm{fus}}$. Representative discharges of individual DTE2 scenarios with the highest q_{DT} are plotted (baseline #99948, hybrid #99912, T-rich #99965, EP #99802, RF #99884, seeded #99621, calibration #99812). The radial distribution of fusion reaction rate for the majority of discharges is largely peaked in the core within $\rho \lesssim 0.4$. But because this area is volumetrically much smaller than the edge, the local fusion gain factor can significantly differ

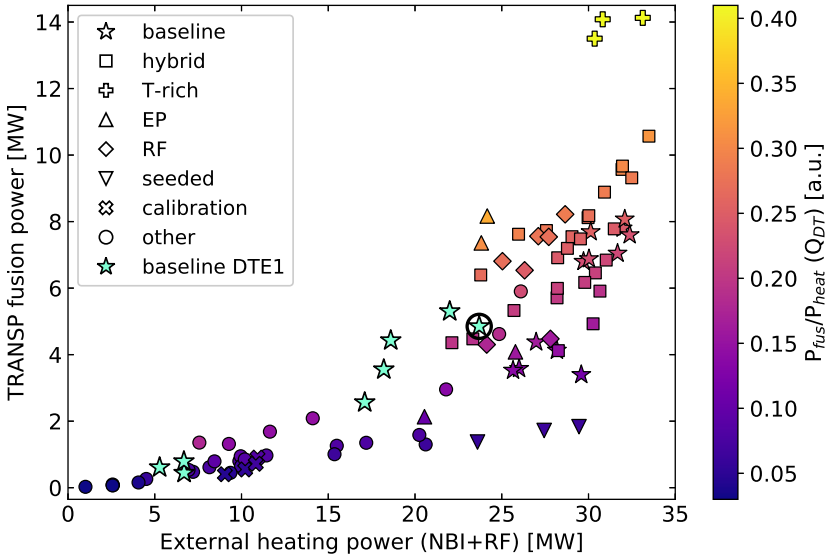

Figure 3: TRANSP computed total fusion power in dependency of the external combined NBI and RF heating power for the DTE2 database. The z-axis (colorbar) denotes the calculated fusion gain factor Q_{DT}, defined as ratio between the achieved fusion and external heating power. TRANSP calculations for a subset of stationary DTE1 baseline discharges are shown (cyan). The scenario type legend notation is used.

from the integrated global Q_{DT} value. Thus one can see that all the highest performing scenarios achieve a peak q_{DT} between $0.6 \sim 0.75$ in the core region, while the lower performing discharges peak at q_{DT} just below 0.2. A clear difference can be seen in the profiles depending on the electron density – both the baseline and seeded discharges with high n_{e} exhibit hollow discharges with peaking at $\rho \sim 0.35$, which is a consequence of broad neutron emissivity profiles and low beam penetration with hollow deposition profiles. In contrast to the one-second-averaged q_{DT} profiles, the highest transient fusion gain, averaged over 20 ms (dashed line), is computed for the EP-hybrid discharge #99802 with a peak value of $q_{\mathrm{DT}} = 0.9$ at $\rho \sim 0.1$. The results agree with the analysis of DTE1 experiments, specifically the record sustained baseline #42982 with and estimated peak q_{DT} of 0.7, but did not repeat the transient $q_{\mathrm{DT}} \gtrsim 1.2$ observed in the hot-ion H-mode discharges that locally exceeded the break-even condition [61].

TRANSP offers insight into the neutron emission characteristics of the modelled discharges, enabling an understanding of the different scenarios' underlying fusion performance drivers. In the left-hand side panel in Figure 5 we display the contributions of the various fusion reaction components to the total fusion power (expanded on in Equation 3), dependent on the total external heating power P_{heat}. We can generally observe that individual fusion components follow a clear power-law trend, which is confirmed by fitted functions (solid lines). It is beam-target fusion (blue) that largely drives JET's D-T performance over the range of heating power. The thermal component (orange) becomes increasingly more prominent at higher heating power, i.e. at ~ 10 MW the BT components is still an order of magnitude larger than TH in average, while the ratio of BT/TH fusion power decreases to around $3 \sim 1$ at heating power above 30 MW. The computed exponents of the fitted functions proportional to $P^{\lambda}_{\mathrm{heat}}$ are $\lambda(TH) = 3.4 \pm 0.6$ and $\lambda(BT) = 2.1 \pm 0.4$ (for fusion power in MW). The beam-beam component (green) remains relatively low in most of the D-T discharges, which is due to the rollover of the D-T cross-section for energetic fuel ions – unlike in deuterium plasmas, there are no D-T fusion performance benefits to evolving an extremely energetic fast ion population. The BB component values display a relatively large spread with respect to the fit due to a

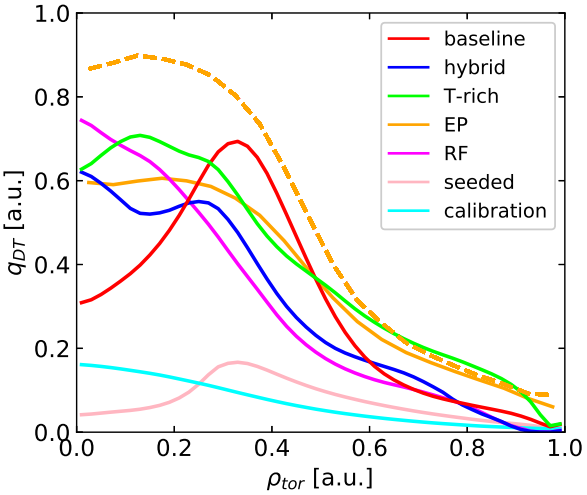

Figure 4: TRANSP computed local fusion gain factor q_{DT} in dependency of the ρ_{tor} radial coordinate (root normalized toroidal magnetic flux $\sqrt{\Psi_{tn}}$). The one-second-averaged results of best performing discharges of individual DTE2 scenarios are shown (solid – baseline #99948, hybrid #99912, T-rich #99965, EP #99802, RF #99884, seeded #99621, calibration #99812), in addition to the highest computed transient q_{DT} (dashed – EP #99802).

strong variation in beam density between the different scenarios, and plateaue at a fusion power of around 200 kW for higher heating power, where they are an order of magnitude or more smaller than both BT and TH, in average contributing to $\lesssim 5$ % to the total fusion power. Similarly the calculated D-D (total reactant energy of 3.65 MeV) and T-T (total reactant energy of 11.3 MeV) fusion power components are low in all discharges due to the low cross-sections compared to D-T, with their combined neutron yield contribution below 1 %.

An important milestone on the path to achieving burning plasma conditions in tokamaks is the development of plasma scenarios in which the majority of fusion interactions is triggered by thermal ions. This would mean that the fuel fast ion concentration in the plasma is low and does not play a significant role either in heating or directly triggering fusion. The heating would ideally be bootstrapped by fusion alpha particles, enabling a high enough electron and ion temperature to sustain the burning reaction. The ratio between beam-induced and thermal D-T neutron yields gives one of the key insights into how JET's various DTE2 scenarios are performing with respect to achieving such conditions, and displays to what degree the fusion performance is dependent on the presence of external plasma heating. We display a graph of the dependency between the computed total fusion power and the (BT+BB)/TH yield ratio for the DTE2 database in the right-hand side panel of Figure 5. The ratio reaches a maximum at around 100 on the right-hand side of the x-axis where discharges with dominating beam-driven fusion are located. On the left-hand side of the graph discharges with equal thermal and beam-induced fusion are clustered. Interestingly one can observe that the distribution of the discharges in the graph indicates that the (BT+BB)/TH ratio is inversely proportional to the external heating power, with the high performing discharges exhibiting larger thermal contributions compared to the lower performing discharges. The baseline discharges have achieved the highest consistent (BT+BB)/TH yield ratio of ~ 1, seen clustered on the top left of the graph. The hybrid discharges exhibit a spread of the yield ratios with the average between $0.8 \sim 0.9$. The database points follow a linear trend in the log-log scaling, which we fitted with a power-law function to obtain a neutron yield ratio exponent of $\lambda(BT/TH) = -0.89 \pm 0.07$ (for fusion power in MW). Assuming the external heating power would reach its nominal installed maximum at 40 MW, the baseline discharges would be expected to reach between

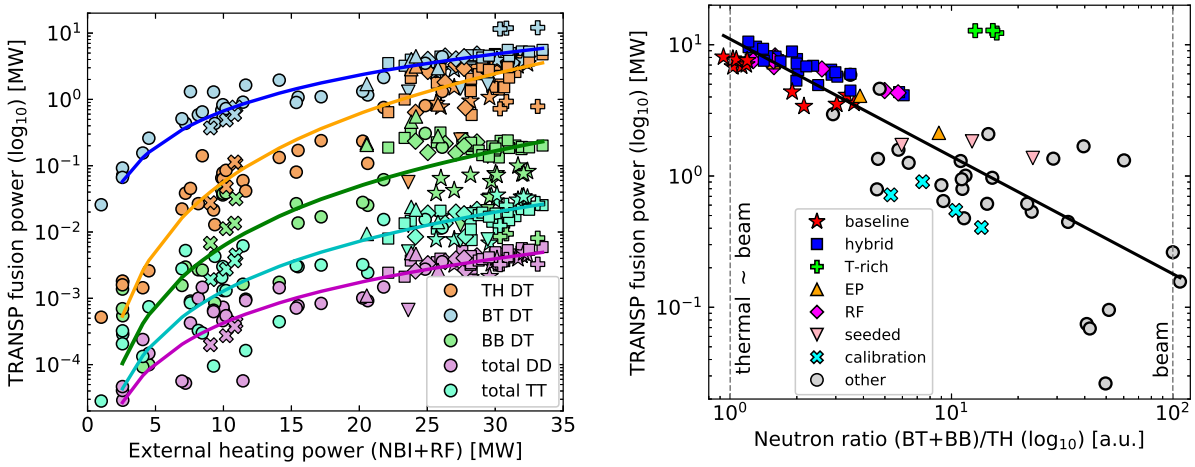

Figure 5: *Left*: computed fusion power components – thermal D-T (orange), beam-target D-T (blue), beam-beam D-T (green), total D-D (magenta) and total T-T (cyan) – in dependency of the external combined NBI and RF heating power for the DTE2 database. The power increase rates for individual components are fitted with a power-law function (solid curves). *Right*: computed total fusion power in dependency of the ratio between the neutrons emitted from beam-induced fusion and thermal fusion neutrons. Discharges with beam-dominated fusion performance are located on the right-hand side of the graph, while the discharges on the left have equal thermal and beam contributions. The distribution is fitted with a power-law function (solid black curve). The graphs share the scenario type legend notation.

13–14 MW of fusion power and an extrapolated (BT+BB)/TH yield ratio of around 0.55, which indicates an approach to a thermal fusion dominated regime. It can be observed that the T-rich discharges do not follow the trend set by the bulk of the high performance discharges, with their record fusion output being highly beam-driven. This is due to the fact the main scenario development branch focused on 50:50 D-T plasma and mixed D-T beam species, in contrast with the T-rich scenario that opted for altered plasma and beam composition to maximize beam performance.

In order to explain the observed discharge distribution with respect to the (BT+BB)/TH yield ratio, we analyse the TRANSP computed electron and ion power balance. In the left panel of Figure 6 we plot the relationship between total ion heating and the yield ratio, with the ratio between core beam and fuel ion densities on the z-axis. We observe that the discharge distribution is similar compared to the right-hand side graph in Figure 5, i.e. the lower performing pulses are in the bottom right, spanning towards the best performing pulses in the top left. This is in line with the observed thermal component increase, confirming that the ability to drive and improve fusion performance is linked to efficient bulk ion heating in $\sim$ 50:50 D-T scenarios. The highest computed ion heating is observed for the baseline, hybrid and T-rich scenarios at around 17 MW, which is approximately half of the total external heating power applied. Interestingly, although the T-rich scenario exhibited one of the highest total ion heating values, and achieved relatively high core T_i, its thermal fusion component remains low – this is a consequence of the plasma being predominantly composed of thermal tritium, with low thermal deuterium concentration, resulting in the density product $n_\mathrm{d}n_\mathrm{t}$ being approximately a factor of 2 lower than that of a 50:50 D-T plasma. The core-averaged relative concentration of the beam population with respect to fuel ions $\langle n_\mathrm{b}/(n_\mathrm{d}+n_\mathrm{t})\rangle$ shows little correlation to the yield ratio or fusion performance and remains below 6 % for the majority of the database. The highest core beam concentration was achieved in the T-rich and EP-hybrid scenarios at above 10 %. At relatively low electron density and high core beam concentration the EP-hybrid discharges display a large total ion heating, resulting in some of the highest on-axis T_i measured in the DTE2 campaign of $\gtrsim$

16 keV. The time-averaged (BT+BB)/TH ratio of these discharges is around 1.6, while discharge #99801 transiently achieved one of the largest relative TH contributions, with (BT+BB)/TH = 0.8.

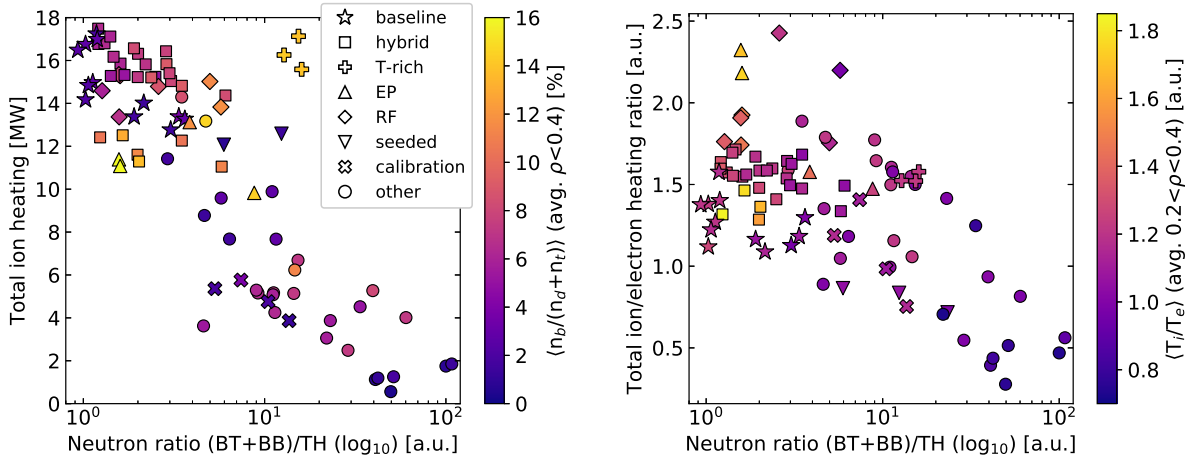

Figure 6: *Left*: computed total ion heating in dependency of the ratio between the neutrons emitted from beam-induced and thermal fusion for the DTE2 database. The z-axis (colorbar) denotes the ratio between the beam and D-T fuel ion density in the plasma core (averaged over $\rho < 0.4$). *Right*: computed ratio between the total ion and electron heating in dependency of the ratio between the neutrons emitted from beam-induced and thermal fusion. The z-axis (colorbar) denotes the ratio between the ion and electron temperature in the plasma core (averaged over $0.2 < \rho < 0.4$). The graphs share the scenario type legend notation.

In the graph on the right-hand side of Figure 6 we look at the decoupling between the electron and ion heating channels. Specifically we plot the dependency between the ratio of total ion over electron heating and the (BT+BB)/TH yield ratio, with the average ratio between core T_i and T_e on the z-axis. It can be seen that there is a clear difference between the low- and high-performing discharges, with the heating ratio rising steadily above unity with increasing fusion output and thermal fusion contribution, reaching maximum values above 2. The average ion over electron core temperature ratio is weakly correlated to the heating ratio – we can observe that the lower performing discharges exhibit $T_\mathrm{i}/T_\mathrm{e} \leq 1$, while the ion temperature starts showing signs of decoupling for higher performing pulses, e.g. the ratio varies between $1.1 \sim 1.3$ for the baseline and hybrid discharges. One can observe an increase in core $T_\mathrm{i}/T_\mathrm{e}$ even within individual scenarios with rising external heating power (moving towards the left-hand side of the graph). We can explain the observations with the following reasoning: with increasing external heating, both the electron and ion temperature rise, but it is T_e that plays the role of the driver due to its linear connection to the beam critical energy, which determines the threshold for the favourable flow of beam energy to the ion channel, and the proportionality of the beam-slowing down time and density to $T_\mathrm{e}^{1.5}$. With increasing beam power the fraction of beam power to the ions increases as well, which in addition to the larger critical energy bootstraps the core ion heating. The temperature decoupling is kept in check by the power balance equipartition term q_ie. Additional favourable mechanisms for the disconnection between the temperatures were recognised, such as the increase in plasma rotation due to increased beam torque and low gas puffing, and its effects on ITG stabilization [62]. We note that the RF scenarios also display a relatively high ion/electron heating ratio and $T_\mathrm{i}/T_\mathrm{e}$ consistently above unity. This can be partially ascribed to the positive effects of various radio-frequency heating schemes – in addition to direct heating of the electron population, an RF fast ion population is formed, initially transferring energy to electrons through collisions. The efficient electron heating raises T_e and the critical energy, and decreases the collisionality, which leads to a formation of a

more energetic fast ion tail. A combination of these effects efficiently bootstraps ion heating, both by the beams as well as the formed energetic RF tail. The two modelled EP-hybrid discharges display a remarkable core T_i/T_e ratio of ~ 1.6, enabled by larger beam penetration due to low electron density and collisionality, and high core rotation. The operational regime relevant for ITER and study fusion pilot plants, exploring burning plasma conditions, is designed to be electron heating dominated with a (BT+BB)/TH yield $\ll 1$. The two conditions have not been simultaneously observed in any DTE2 JET discharge and appear to be mutually exclusive for the analysed plasma condition range – as observed in Figure 6 the electron heating dominated discharges (located on the right-hand side of the two graphs) display a low-performance, predominantly driven by beam-induced fusion with TH contributions $\lesssim 5$ %. On the other hand the best performing discharges follow a clear trend of rising ion heating in favour of the electron channel with increasing external heating power, reaching an average total ion/electron heating ratio of ~ 1.5.

In the left-hand side graph of Figure 7 we look at the relationship between the fitted toroidal rotation frequency averaged in the core ($0.2 < \rho < 0.4$), and the effective core collisionality that is proportional to $\langle n_e \rangle / \langle T_e^{1.5} \rangle$, volume averaged within $\rho < 0.5$. The collisionality of the majority of best performing pulses is relatively low, i.e. between the values of 2 – 5, which is in agreement with the conditions that are needed to drive a high T_i/T_e ratio. Such an example are the EP-hybrid discharges which, at relatively low density and high T_e exhibit the lowest collisionality of the database, in addition to a combination of a large core rotation and core beam heating. A large portion of the lower performing pulses display $\langle \nu_{eff} \rangle$ above 5, reaching maximum values of around 15. Core rotation in principle inversely depends on plasma density and collisionality, which is demonstrated with the $\Omega_t(\langle \nu_{eff} \rangle)$ trend in the graph. At low collisionality the edge-core rotation coupling is weak, which in combination with the presence of axis beam momentum deposition can result in high core rotation, like seen in some hybrid and EP discharges. In the baseline discharges the higher pedestal density results in increased beam angular momentum deposition at the edge, increasing the edge rotation frequency. A slightly higher collisionality in these discharges enables higher momentum transfer to the core, which in combination with particle fuelling effects helps keep the rotation relatively high [62]. The rotation angular frequency thus has a dependency on the scenario type, with the highest fusion output discharges displaying values above $\sim 7{\cdot}10^5$ rad/s. Seven database discharges do not have available rotation data which is due to a lack of CX measurements, all of them lower-performing. A finite Ω_t also directly affects the beam-target fusion reactivity, due to the fact that the relatively ion velocity term, introduced in Equation 2, changes. Whether $\mathbf{v}_{rel}$ increases or decreases depends on the passing or counter-passing nature of the target ion. TRANSP and ASCOT simulations have shown that the effect of including rotation profiles on the neutron yield was up to 10 % in deuterium high performance plasmas, with the addition of rotation generally resulting in a net yield decrease [63]. Further investigations into the effects of rotation in high performance D-T plasmas is presented in [28]. On the z-axis we display the ratio between the beam deposition source in the core (at $\rho = 0.25$) and at the edge (at $\rho = 0.8$), which is a measure of the beam deposition profile peakedness. There is no clear correlation with the collisionality, but there is an observable dependency on the electron density, resulting in differences between the high performance scenarios. The baseline and seeded discharges with the highest n_e in the campaign have the lowest beam peakedness with values below 1, meaning that the fast beam ion deposition profiles are hollow and peak at the edge. On the other hand the hybrid discharges display deposition ratio values of $\gtrsim 1.5$ at lower electron densities. The T-rich experiments have some of the most peaked profiles, owing not only to hybrid-like n_e, but also to the fact that the injected beams are pure deuterium, which has a larger penetration depth due to its lower mass – a single-isotope beam configuration was used for other pulses with the highest peakedness as well.

The graph on the right-hand side of Figure 7 displays the dependency of the volume averaged ($0 < \rho <$

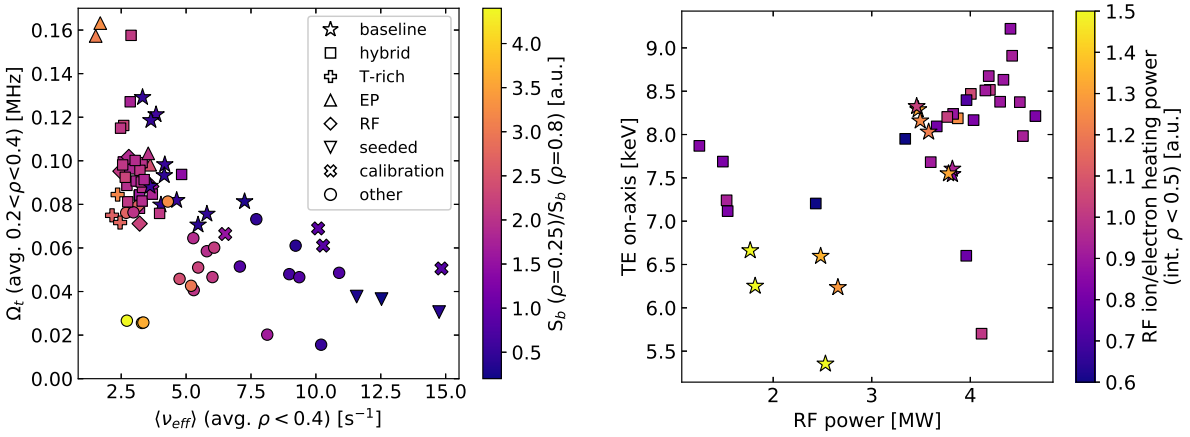

Figure 7: *Left*: fitted core-averaged toroidal rotation frequency in dependency of the effective collisionality for the DTE2 database. The z-axis (colorbar) denotes the ratio between the total beam deposition source in the core ($\rho = 0.25$) and at the edge ($\rho = 0.8$). *Right*: On-axis electron temperature fits in dependency of the injected RF power for baseline and hybrid DTE2 discharges only. The z-axis (colorbar) denotes the ratio between the ion and electron RF heating power integrated within $\rho < 0.5$. The graphs share the scenario type legend notation.

0.5) core electron temperature on the injected RF power, with the colour-coded symbols indicating the ratio between ion and electron RF heating power. The latter includes both direct RF wave absorption and collisional heating by minorities to both channels. The data shown in the graph is based on a reduced set of baseline and hybrid discharges only. The subset was chosen because the H RF minority scheme was consistently applied in the scenarios, using a relatively unchanged minority concentration of $X[H] \sim 2$ % ± 1 %, at similar NBI heating power. In other scenarios, e.g. T-rich and RF, different minority species and concentrations were employed, rendering the discharges unsuitable for this comparison. The plot shows that the core electron temperature increases with RF power. In both baseline and hybrid discharges it can be seen that the central T_e increases by around 1 keV per ~ additional 2 MW of RF power applied. In absolute terms the average value of the lowest RF power injected is around 2 MW, while the maximum is approximately 4.5 MW. The baseline discharges exhibit a consistently higher ratio of ion to electron heating, compared to the hybrid discharges. In the baseline scenario the ratio of ion over electron core heating consistently reaches values between 1.2 ~ 1.5, while the hybrids display a lower spread with an average value of around 0.85. The hybrid discharges achieved core electron temperatures higher than those of the baseline shots in average at lower RF power, however the latter seem to exhibit a steeper T_e rise rate. An interesting observation is that at low P_{RF} and T_e the ion over electron heating is calculated to be higher than at high P_{RF} and T_e, which is contrary to what is expected. Namely as the critical energy of fast H ions decreases with dropping T_e, one would anticipate that if the minority population is accelerated to the same energy more power would flow to the electrons. On the contrary the hybrid discharges display a weak increase of ion over electron heating with at larger RF power. In addition to the fundamental H minority RF heating in the selected pulses, a part of the RF power is absorbed on fast D-beam ions as well, which are accelerated via the second harmonic Doppler broadened resonance. Acceleration of energetic D or T ions by RF waves, i.e. so-called synergistic effects, has been shown to improve D-T fusion performance to some extent [64, 31]. For instance, extremely efficient ion heating was demonstrated in dedicated T-rich experiments, with RF power densities on bulk and fast ions being a factor of 2–4 higher than those deposited on electrons. Other RF heating schemes which were employed in JET D-T discharges include

fundamental resonance on D ions, ^{3}He minority and second harmonic T heating [33], as well as the 3-ion scheme. In the latter a resonant ion-ion hybrid layer is formed due to the presence of a minority ion species with an intermediate charge-to-mass ratio with respect to the majority D-T ions, in this case JET's intrinsic metal wall impurity ^{9}Be [65]. All of the above-mentioned schemes have certain advantages and disadvantages. For instance, the advantage of fundamental D heating and second harmonic T heating is that the RF waves directly heat the fusion reactants in a D-T plasma, impacting fusion performance. However the D-T reactivity for fast-thermal ion interactions peaks at around 130 keV for deuterons and 190 keV for tritons, after which it decays and reduces by approximately a factor of 2 at energies of 300 keV. This means that a fine balance needs to be struck between efficiently RF-accelerating ions, ensuring both bulk and fast ion heating, yet not producing a fast ion population that is too energetic, which could overshoot the maximum of D-T reactivity. In highest-performing deuterium plasmas the direct contribution of RF fast ions to fusion performance was found to be between 10 $\sim$ 15 %, with the beam synergy effect having a large role due to a monotonously increasing D-D cross-section [42, 15, 18, 66]. In D-T plasmas the direct performance contribution of RF is found to be smaller, varying between 3 $\sim$ 5 % for synergy fast ions in baseline and hybrid discharges [64], to approximately 10 % for fundamental D-majority heating in the T-rich experiment, discussed in more detail in Section 4.

Next an analysis of the time evolution of fusion performance for two representative high-power discharges is presented, the baseline #99863 and hybrid #99950. These two discharges were chosen because both were performed at a fuel mixture close to 50:50 D-T, displayed similar T_e and T_i at the start of the heating phase, and employed NBI and RF heating with matching power, both using the H minority RF scheme. We focus on the differences in the evolution of their neutron yields, caused by discrepancies in plasma conditions, from the beginning on the heating phase to the point of reaching steady-state performance. Figure 8 displays a comparison of selected plasma parameters, from top to bottom neutron yield, external P_{heat}, core line-integrated n_e, and on-axis T_e and T_i, with a shared y-axis between the horizontal graph panels.

Baseline: the time interval [47.55, 50.4] s from the beginning of NBI heating to a point of performance deterioration preceding a disruption is shown. After the beam is turned on the BT fusion component starts to rise and remains dominant for one second. It is the n_e and T_e that govern the fusion performance conditions in this phase. One can see that there is a relatively large increase in n_e at the beginning, limiting the beam penetration depth and the rise rate of the BT component. The T_e is dependent solely on NBI power at the beginning, with the its rise rate relatively low. Due to the dominant inverse power-dependency of collisionality to T_e the beam energy distribution is slowly becoming more energetic, favourable for fusion, which in combination with increasing ion density drives the beam-induced yield increase. It is not until $\sim$ 48.5 seconds that T_i also starts increasing, driving the TH yield component. This occurs due to a combination of factors – the RF heating is turned on at 48 seconds, which supports the power flow into the electron channel, bootstrapping T_i trough an increase in critical energy. There is also a drive in bulk ion heating through fast H minority slowing-down. Collisionality is still not stabilized and is not low, therefore the RF tail is not expected to be highly energetic. There is an additional effect of RF power deposition on D-NBI ions through the Doppler-shifted second harmonic resonance, boosting BT fusion directly by energizing beam ions and contributing to bulk temperature increase. A large sawtooth event at 48.9 s strongly affects T_e and caps its steady-state on-axis value to $\sim$ 8 keV. This also slows the rise rate of the total neutron yield through the effect on beam density, core fast ion redistribution, and indirectly through an induced decrease in critical beam energy and ion heating. Maximum performance is achieved at 49.6 s, when the TH and BT components are approximately equal. The electron density control mechanism was not adequate in baseline D-T discharges, with n_e increasing throughout at a linear rate. This has been postulated to coincide with a weakening of ELM activity, crucial for density control and impurity flushing, which lead to impurity

accumulation, radiation increase and a subsequent disruption [23]. One can observe that both electron and ion temperatures start decreasing after 49.5 s, meaning that only a quasi-steady-state was reached, which is a consequence of a combination of the density effect and detrimental MHD activity, e.g. sawteeth and neoclassical tearing modes.

Hybrid: the time interval [47.0, 50.0] s from the beginning of NBI heating to reaching flat-top performance is shown. The hybrid discharge starts at a low n_e at the beginning of the heating phase, with an initial deep beam penetration. This results in a strong drive of T_e rise, which at a $\sim$ constant n_e (initial 500 ms) causes the collisionality to decrease. These are favourable conditions for an efficient evolution of an energetic RF tail, which contributes to both a further increase of T_e, as well as T_i. Several 100 ms into the heating phase, the ion heating is bootstrapped with the T_i increasing at a high rate of approximately 7 keV in 500 ms. The efficient triggering of the electron and ion heating channels is one of the main differences compared to the baseline scenario, with the hybrid pulse reaching levels of fusion performance close to its maximum after approximately one second, a rate twice as fast as the baseline. The hybrid TH yield rises in unison with the plasma density, which is the dominating term in the reaction rate calculation, as T_i is already high. The BT component reaches steady-state when both the electron density and temperature flatten out, equilibrating the effects of beam penetration and slowing-down time on beam density. The high performance is sustained for $\sim$ 3 s with good n_e control, after which the T_e profiles became hollow due to impurity accumulation, which lead to increased neoclassical tearing mode activity and performance deterioration [26]. Compared to be baseline discharge the steady-state yield was dominated by the BT component, with the TH approximately 25 % lower. The hybrid pulse #99950 achieved a record integral fusion energy output of 45.8 MJ for a 50:50 D-T plasma with mixed D-T beams. One can observe the benefits of an elevated-q sawtooth-free regime with no negative effects on core T_e and fast ion redistribution. Comparing the flat-top core T_e and T_i, we see that the hybrid pulses achieved $\sim$ 1 keV larger values in average. Interestingly the maximum absolute yield of the TH component is comparable in both cases.

One of the main aims of the work presented in the paper is assessing the fidelity of interpretive TRANSP calculations of the fusion power output, and comparing these to JET's absolutely calibrated neutron yield measurements. In Figure 9 we present the relationship between the ratio of TRANSP total neutron yield calculations and absolutely calibrated measurements (calculation/measurement -1 in %), and total external heating power. We compare the neutron yield discrepancy distribution for both the JET-ILW D (blue) and DTE2 (gold) discharge databases, in addition to plotting the mean of the computed ratios (bin width 5 MW). The deuterium discharge database shows good agreement between the measurements and calculations over the whole range of heating power, within the combined experimental and computational uncertainty of ± 25 % denoted with the grey dashed lines. A difference between lower and higher performing discharges can be observed, with the heating power threshold for the grouping being around 20 MW – namely one can observe that the spread of the computed discrepancy is higher for low-power discharges with an increased mean of $\sim$ +15 % (black dashed line), while the best performing discharges, spanning a range of heating power of more than 15 MW, show an excellent agreement with measurements, with the mean discrepancy being $\lesssim$ +5 %. Interestingly this finding does not agree fully with other previous studies of fusion performance modelling in deuterium plasmas on large databases [12, 13], where a systematic over-prediction of TRANSP calculations of up to +50 % was reported. The DTE2 database yield discrepancy similarly exhibits a difference between plasmas heated with either above or below $\sim$ 20 MW of power. However in D-T calculations for discharges with relatively low performance systematically over-estimate the fusion power measurements by approximately +40 %, while the discrepancy mean falls to around +10 % for the highest performing discharges, again exhibiting a good match with the measured neutron yield. Interestingly, while the increased heating power mainly corresponds to high performance, the Ne-seeded discharges perform poorly for high

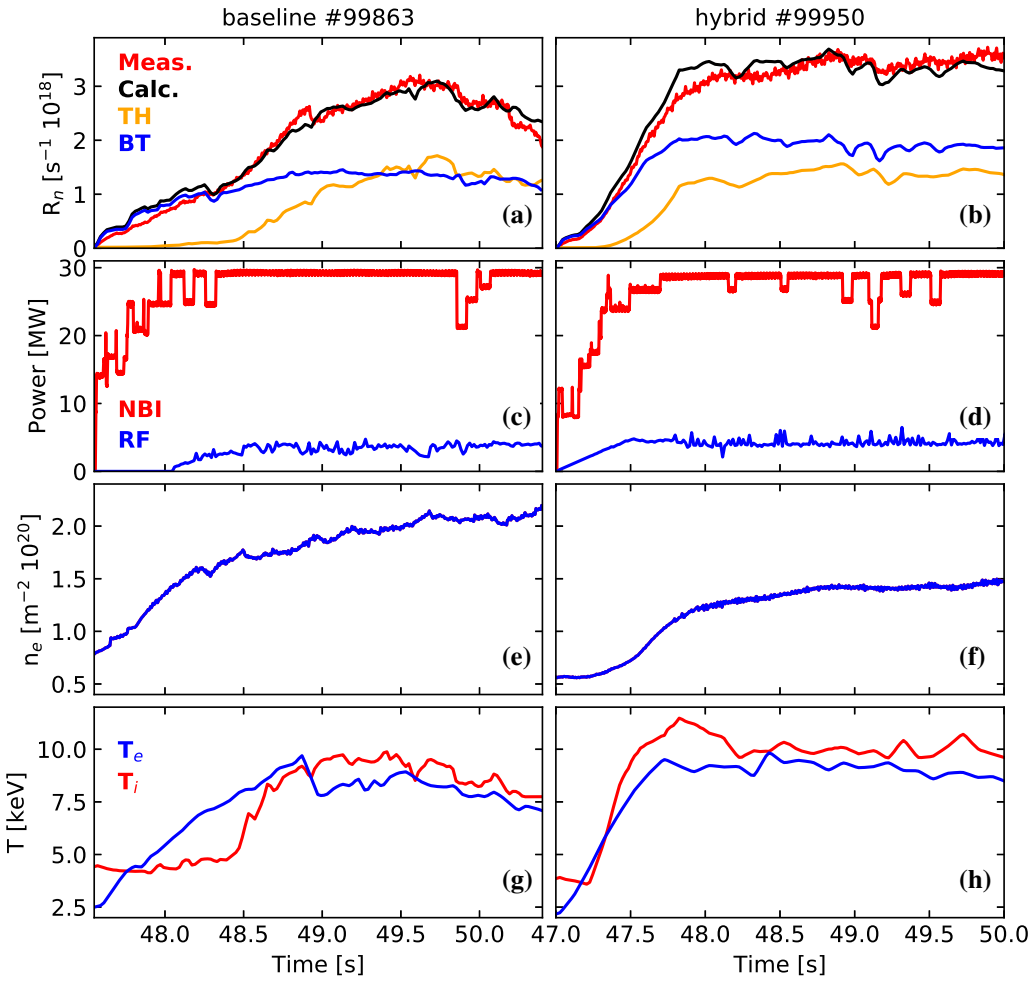

Figure 8: Comparison of plasma parameters for the baseline #99863 (*left*) and hybrid #99950 (*right*) D-T discharges. Panels *(a)* and *(b)* display a comparison between the time-evolved total neutron rate measurement (red) and the TRANSP calculation (black), which is further split into the thermal (orange) and beam-target (blue) components. Panels *(c)* and *(d)* show the NBI (red) and RF (blue) power waveforms, with the core line-integrated electron density measurement shown in panels *(e)* and *(f)*. The on-axis electron (blue) and ion (red) temperature fits are shown in panels *(g)* and *(h)*.

heating levels (as observed in Figure 3) and display uncharacteristically high yield discrepancies of around +60 %. The observed correlation between the calculation/measurement neutron yield discrepancy and discharge performance for both D-D and D-T plasmas is similar to the relationship observed in the analysis of fusion output contributions from different fusion components, as seen in the right-hand side graph of Figure 5. Indeed if P_{heat} on the abscissa of Figure 9 is replaced by the ratio between beam-induced and thermal fusion, plotted in Figure 10, the discharges with larger average discrepancy cluster towards the right-hand side of the graph. This means that a majority of the pulses for which the fusion power calculation was over-predicted exhibit a beam-driven fusion performance, with a (BT+BB)/TH ratio of $\gtrsim 6$.

The DTE2 data thus suggests that the calculated beam-target fusion component might be systematically overestimated – possibly this effect is emphasized in lower performing discharges due to the fact that BT neutrons comprise more than 90 % of the total neutron yield, and due to plasma conditions governing the

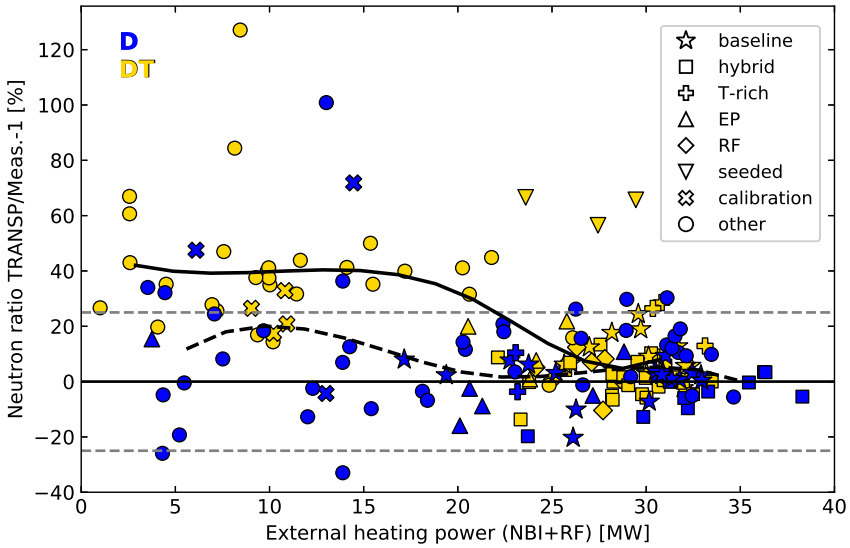

Figure 9: Comparison of the ratio between TRANSP neutron yield calculations and absolutely calibrated measurements (calculation/measurement -1 in %) for JET-ILW D (blue) and DTE2 (gold) discharge databases. The total NBI and RF external heating power is plotted on the x-axis. The mean of the neutron yield ratio is shown for D (black dashed curve) and D-T (black solid curve) discharges. The grey dotted lines denote a ± 25 % uncertainty of the neutron yield ratio. The scenario type legend notation is used.

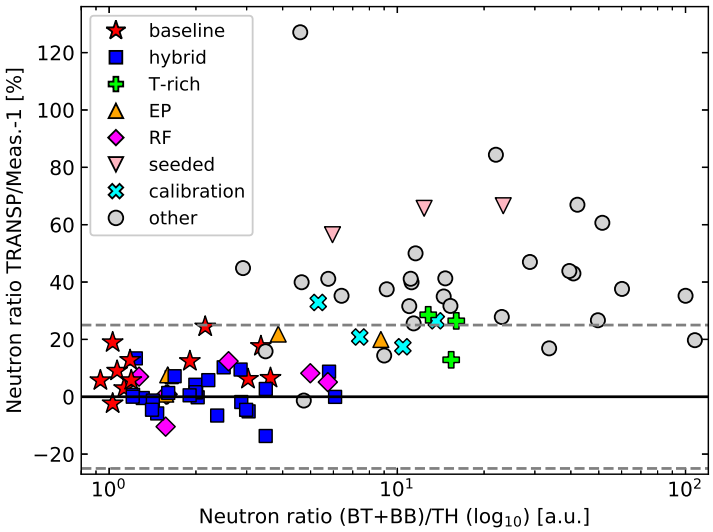

Figure 10: Ratio of TRANSP neutron yield calculations and absolutely calibrated measurements (calculation/measurement -1 in %) in dependency of the ratio between the neutrons emitted from beam-induced and thermal fusion for the DTE2 database. The grey dotted lines denote a ± 25 % uncertainty of the neutron yield ratio. The scenario type legend notation is used.

behaviour of beam fast ions. The beam-induced D-T fusion rate is computed through the following two terms of Equation 3: $n_{\mathrm{db}} n_{\mathrm{t}} \langle \sigma v \rangle_{\mathrm{BT}}(D \rightarrow T) + n_{\mathrm{d}} n_{\mathrm{tb}} \langle \sigma v \rangle_{\mathrm{BT}}(T \rightarrow D)$, which represent deuterium and tritium beams impinging on a thermal target of the opposite fuel ion, respectively. Trying to understand where the beam-target reaction rate might be overestimated, we scrutinize the terms' three major dependencies:

thermal ion density, beam ion density, and the beam-target reactivity. The thermal densities are relatively well defined through a combination of electron density, ZEFF and isotope composition measurements and are unlikely to contribute to the discrepancy, which will be expanded on in Section 3.2. The beam density n_b is computed with the NUBEAM module through Monte Carlo particle tracking, however to discuss potential sources of systematic error we expand on the evolution of the beam ion population in a classical way. It is obtained by integrating the analytically or numerically obtained fast ion distribution function $f_b(E_b, \xi)$ in energy E and pitch angle ξ, and is related to the beam slowing-down calculation:

$$n_b \propto \int_0^{E_0} \int_{-1}^{1} f_b(E_b, \xi) \sqrt{E}\, dE\, d\xi, \text{ with } f_b(E_b) \propto \sum_i \frac{S_i \tau_s}{\left(1 + \left(\frac{E_{crit}}{E_{b,i}}\right)^{1.5}\right)}, \tag{4}$$

where i stands for the full, half and third-energy beam ions, S_i the beam particle source rate, τ_s the Spitzer slowing-down time, and E_{crit} the beam critical energy. The beam source term is defined by the particle deposition profiles and depends on the beam species characteristics and plasma density – these are well defined, with the shape of the deposition profiles reliable. The amplitude of the particle source on the other hand might be affected due to beam power calibration uncertainty [16], assessed in Section 3.2. τ_s is inversely proportional to $n_e/T_e^{1.5}$ and consequently the effective collisionality. We've seen in the left-hand side graph of Figure 7 that $\langle \nu_{eff} \rangle$ shows a dependency on the fusion performance, with a majority of the lower performing discharges displaying higher collisionality values above ~ 5. Additionally the slowing-down time depends on the electron Coulomb logarithm, the values of which vary by only several percent around an average of approximately 17.5 for the whole database. E_{crit} is linearly dependent on the electron temperature and is not expected to introduce significant uncertainty. To summarize, while the calculated beam density does not show a dependency on the (BT+BB)/TH yield ratio, as seen in Figure 6, the beam slowing down distribution does depend on input or calculated terms that are uncertain, i.e. prescribed beam power and the computed collisionality. An additional source of uncertainty in n_b stems from the fact that NUBEAM takes into account classical and neoclassical fast ion evolution effects, but it does not describe anomalous transport, owing to turbulence and MHD activity. While this has been shown to cause computational neutron over-prediction due to a strong suppression of beam-induced fusion in the presence of resonant MHD instabilities, e.g. MAST, DIII-D and ASDEX Upgrade [67, 68, 69, 70], it has not been unambiguously shown that similar phenomena govern the transport of fast particles in JET. Such studies have predominantly been done for deuterium-majority plasmas – for example a study of JET's 2003 trace tritium experiments in which a T beam was injected into a pure D plasma found an overestimation of the computed fusion power for both the D-D and D-T neutron dominated plasmas. To obtain a match in the neutron rates a relatively large fast ion anomalous diffusion D_a between 5 and 10 m^2/s was applied. We've applied the same level of radially-independent D_a to a selection of the D-ILW database discharges with beam-driven fusion performance, that overestimated the D-D neutron yield measurements – see D calibration scenario discharges in Figure 9. It was found that at $D_a = 5$ m^2/s the beam density was significantly reduced compared to the reference case without anomalous transport – n_b was reduced by a factor of 4 in the core, while the volume-integrated value reduced by more than a factor of two. With this level of anomalous diffusion applied the n_b radial profile became extremely flat and lost all core peakedness, with the total neutron rate decreasing by around 40 %. While this yield decrease compares well to the observed over-prediction, the effects of changes in beam density on calculated profiles of neutron emissivity and fast ion losses are substantial not corroborated by diagnostics measurements. There is also no indication that MHD activity effects could exhibit a similar dependency on the external heating power as the one observed in the neutron yield discrepancy. On the contrary, the activity of fast ion driven modes like fishbones is expected to increase with rising beam power, and prominent tearing mode activity is observed

in some high performing discharges. An analysis of JET's MHD activity based on measurements of a high resolution toroidal magnetic probe array published in [12], revealed no correlation between mode activity and level of neutron yield reproduction. The redistribution of fast ions due to sawteeth and its effect on the neutron yield have been studied at JET [71], however this is a transient effect with the sawtooth-cycle generally long enough compared to the average fast ion slowing-down time ($\lesssim$ 100 ms), to allow for the beam ions distribution and neutron yield to reach steady-state. The final term defining the beam-target D-T fusion yield is the reactivity $\langle\sigma v\rangle_{\mathrm{BT}}$. The cross sections were based on the thoroughly validated Bosch-Hale parametrization [72], so the potential uncertainty lies in the relative ion velocity term – the bulk thermal ion temperature contributes relatively little to the total velocity, therefore the reactivity has a low sensitivity to uncertainty in T_{i}. The energy distribution of the beam ions is the term that has the largest uncertainty weight in the reactivity calculation, with the potential sources of uncertainty similar to the ones discussed for n_{b}. Additional investigation into the effects of MHD instabilities on the redistribution of fast ions, and consequently the beam-target neutron yield, could be made by coupling of orbit tracking and MHD codes, such as [71, 73, 74], to better describe the radially and energetically localized nature of anomalous diffusion. Experimental validation of fast ion transport at JET is difficult because the fast ion density is not measured by techniques applied at other tokamaks, e.g. the FIDA system measuring D_α light emission from neutralized fast ions [75, 76].

3.2. Computational uncertainty

To understand relatively how large the observed discrepancies between the calculated and measured neutron yield are, the uncertainty of the TRANSP interpretively computed fusion power was calculated. This was done by varying a set of most prominent input parameters by ± 10 %, i.e. the electron density, electron and ion temperature, angular rotation frequency, NBI power and the D-T thermal fuel mixture. Three representative discharges were chosen for the analysis, namely the high-performing baseline #99863 and hybrid #99950 discharges, both with slightly different fusion drivers, and the lower performing calibration discharge #99812, all with mixed D-T beam injection. The latter exhibits plasma parameters representative for beam-driven fusion performance and the calculated fusion power over-estimated by an average of 25 %. Additionally, this type of discharge is used in the cross-calibration of fission chambers against the time-integrated neutron yield measurements by the foil activation system [77].

We first present the sensitivity study for one of the most important D-T plasma parameters, the fuel mixture – on the left-hand side graph in Figure 11 the dependency between the yield discrepancy ratio and on-axis $n_{\mathrm{d}}/(n_{\mathrm{d}} + n_{\mathrm{t}})$ is shown. Importantly, no correlation between the two can be seen, with the majority of the pulses performed within a $n_{\mathrm{d}}/(n_{\mathrm{d}} + n_{\mathrm{t}})$ ratio interval of $0.4 \sim 0.6$, with an approximately 5 % deviation from the 50:50 mixture toward the more fusion favourable T-rich composition. As described in Section 2 the initial composition of the plasma was taken from the edge residual gas analysis and extrapolated to the core, based on impurity and beam dilution. It was found that the computed core mixture matched with the fixed edge value within a couple of percent for the majority of the pulses, indicating good mixture control and fast core isotope mixing. The edge mixture boundary condition was varied by ± 10 % and ± 20 % for the selected discharges, in order to study the effect on the computed fusion power. The results are shown in the right-hand side panel of Figure 11, where the reference TRANSP runs are encircled. One can observe all three plasma shots show a similar trend of increasing fusion power as the fuel mixture is tritiated more, and the opposite for a dominant deuterium mixture. The three scenarios show different rates of change due to their individual dependency of the performance to the beam-driven over thermal fusion ratio. One can observe that with a dominating beam-target component, such as the calibration discharge, the relation between the rate of fusion power change and the fuel mixture is linear in the vicinity of the 50:50 composition. This is because the benefit of injecting deuterium beams into a T-rich plasma is significantly

larger than the decreasing contribution of the thermal fusion proportional to the thermal ion density product due to a decreasing deuterium bulk concentration. On the other hand the baseline discharge's performance is dominated by thermal fusion, which means that the benefits of the D beam → thermal T cross section is diminishing compared to the diminishing thermal density product, reaching a plateau at around $n_\mathrm{d}/(n_\mathrm{d}+n_\mathrm{t})$ ~ 0.4. However in all cases the relative change of the fusion power due to changes in the fuel mix is relatively small, reaching values of around ± 2 % at a 10 % composition variation.

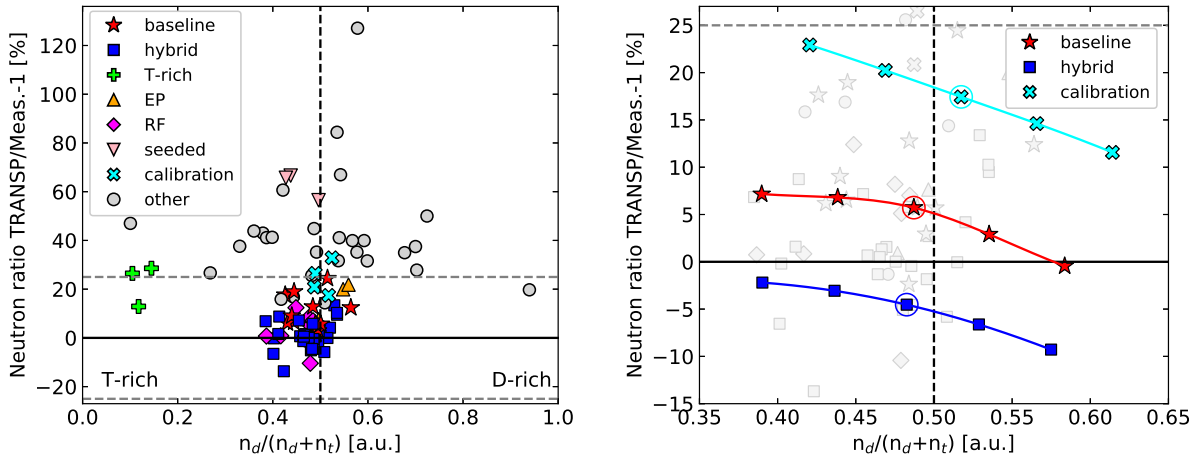

Figure 11: *Left*: ratio of TRANSP neutron yield calculations and absolutely calibrated measurements (calculation/measurement -1 in %) in dependency of the ratio between on-axis deuterium and total fuel ion density. Deuterium-rich discharges are located on the right-hand side of the graph, with the T-rich on the left. *Right*: zoom-in of the left panel graph, displaying the fuel ratio sensitivity calculation. The fuel composition of three D-T discharges – baseline #99863, hybrid #99950 and calibration #99812 – was varied by ± 10 and ± 20 %. The graphs share the scenario type legend notation.

The plasma parameters input into TRANSP as fits of measured data were varied within ± 10 %, which is a 1σ estimate of the uncertainty due to measurement scatter. While this is a good approximation for a majority of the fits, it can be considered a lower estimate for the core ion temperature due to the scarcity of core CX measurements, which strongly depends on the plasma scenario. The nominal uncertainty of the beam power is cited as ± 10 % for both D and T beam species, and strongly depends on the beam calibration effort [16, 78]. In Table 1 a summary of the sensitivity study is presented, with the variation in neutron yield dependent on the corresponding plasma parameter perturbation. In the final row the total uncorrelated uncertainty for individual scenarios is computed as $\sqrt{\sum \sigma_\mathrm{i}^2}$, where we assume that there is no correlation between the measurements' experimental uncertainties obtained with independent diagnostics. The largest three contributors to the total computational uncertainty are denoted in bold. We can observe that n_e is an important parameter for the calculation of fusion power in both the baseline and hybrid discharges, with a 10 % density change resulting in almost the same variation in the yield – in the former predominantly because the thermal fusion rate depends on the thermal ion density product. In the hybrid discharge this is due to a combination of an effect on the thermal density, playing a role in both thermal and, linearly, in beam-target fusion, as well as beam penetration. Interestingly the calibration discharge shows a weak sensitivity to variations in n_e, a consequence of the performance being driven by the beam-target component. Namely the linear dependency of the BT fusion rate to thermal ion density is overpowered by the beneficial effect of improved beam penetration, higher core beam density and longer beam slowing-down times boosting the fusion reactivity. The variation in T_e shows little effect on the baseline and hybrid discharges because

the core T_e values are already relatively high, as shown in Figure 8, with the $\sim$ 2.5 % R_n change due to beam-slowing down. Again owing to the beam-target dominance the T_e variation in calibration discharges will trigger changes to the beam slowing-down dynamics through collisionality, indicated in Equation 4, resulting in changes of the total R_n of $\pm$ 9 %. The largest effect on baseline's fusion output is triggered by perturbing T_i, reaching a maximum of 18 % due to its strong dependency on the TH yield. The impact on the hybrid performance is similarly high at just below 15 %, while the calibration discharges show a weaker response at around half the values of the other scenarios, mostly stemming from the effect on the computed $\langle\sigma v\rangle_{BT}$ reactivity for the low energy part of the beam ion distribution. The perturbation of plasma rotation input does not propagate to large discrepancies in R_n, with an average scenario-independent value of around 1 %. The uncertainty of the beam power on the other hand has a large effect on the total yield calculation – since this is an interpretive analysis the change in beam power will not propagate to kinetic profiles, and will thus only enter the fusion power calculation through the beam source strength term, illustrated with Equation 4, affecting the BT and BB components. Baseline and hybrid discharges record an approximately 15 % change in the total yield, rivalling the importance of T_i, while the effect on the calibration discharge is extremely large. The $\sim \pm$ 30 % change originates from the effects on the evolved beam ion density profile, which is similar for the reference and perturbed cases within ρ = [0.7, 1.0], but it starts to deviate towards the plasma core reaching a difference of 25–30 % on-axis. Additionally we've varied the impurity composition of the baseline case from the original 1 % Be, 0.01 % Ni and 0.48 % Ne to $\pm$ 0.75 % Be as the main core impurity dilutant. The resulting effect on the quasi-neutrality and ZEFF calculation was absorbed by Ne, the concentration of which changed by $\mp$ 0.1 %. The core dilution change resulted in a total yield variation of around $\pm$ 3.5 %, which is expected to be equivalent in the hybrid case due to a similar response to n_e perturbation, and small for the calibration discharge. Summing up the contributions yields a total computational uncertainty estimate for the fusion power of approximately 25 % for the baseline and hybrid and 35 % for the calibration discharges. This shows that the uncertainty of D-T neutron yield calculations based on validated data is much larger than the experimental uncertainty of the absolute neutron yield measurements, estimated to be below $\lesssim$ 10 % [7]. In addition the calculational uncertainty is found to be dependent to the mechanisms driving fusion performance and thus the plasma scenario.

Table 1: Summary of plasma parameter sensitivity study for three D-T discharges – baseline #99863, hybrid #99950 and calibration #99812 – to determine the total uncorrelated uncertainty of the computed fusion power (proportional to total neutron rate R_n). Electron density n_e, electron temperature T_e, ion temperature T_i, toroidal rotation frequency Ω_t, NBI power, and D-T fuel ratio $n_d/(n_d + n_t)$ were varied by 10 %, with the scaling constant being time and radius independent.

Discharge → Parameter variation ↓	baseline #99863 R_n variation [%]	hybrid #99950 R_n variation [%]	calibration #99812 R_n variation [%]
n_e ± 10 %	**+9.5 / –9.2**	**+9.9 / –9.1**	–0.9 / +1.1
T_e ± 10 %	+2.3 / –3.4	+2.5 / –2.7	**+8.8 / –9.0**
T_i ± 10 %	**+18.0 / –16.1**	**+14.6 / –13.1**	**+6.8 / –5.4**
Ω_t ± 10 %	–1.1 / +0.4	–1.1 / +0.9	–1.3 / +1.5
P_{NBI} ± 10 %	**+14.2 / –13.2**	**+15.5 / –13.6**	**+33.7 / –28.2**
$n_d/(n_d + n_t)$ ± 10 %	–2.7 / +1.0	–2.2 / +1.5	–2.4 / +2.4
Uncorrelated total uncertainty	**+25 / –23**	**+24 / –21**	**+36 / –30**

3.3. Fusion alpha particles

We briefly report on an important physics insight of JET's DTE2 experiments, the alpha particle physics. Because the fusion alpha source strength is linearly proportional to the neutron yield, the fidelity of alpha particle effects modelling is related to our capability to reproduce the measured fusion performance. Having validated the computed neutron yield, we can analyse the trends of alpha power balance, and assess the alpha pressure – both of these quantities are relevant for extrapolation of conditions to burning plasmas of future fusion reactors, where we will need to understand the role alphas play in plasma self-heating and in driving plasma instabilities such as Alfvén eigenmodes. In the left-hand side panel of Figure 12 we present the relationship between the alpha heating power and the external plasma heating power. The power balance is split into the electron (blue) and ion (red) channels, both exhibiting a power-law dependency on the increasing heating power, correlated to the fusion power trend shown in Figure 3. One can observe that for maximum achieved values of P_{heat} above 30 MW the alpha heating of electrons reached levels of around 1–2 MW, while the ion heating was computed to reach a high of 200–300 kW. The computed exponents of the $P_{\mathrm{heat}}^{\lambda}$ dependency are $\lambda(\alpha_{\mathrm{e}}) = 1.9 \pm 0.4$ for electrons, and $\lambda(\alpha_{\mathrm{i}}) = 2.4 \pm 0.5$ for ions, with the ratio between electron and ion heating from alphas being $\lesssim 10$ for the high performing discharges and decreasing. On the right-hand side graph of Figure 12 we plot the dependency of the ratio between the total alpha and beam ion heating, and P_{heat}. It can be seen that there is a strong and favourable increase in the relative contribution of alphas to the ion heating, however for the highest performing T-rich discharges, with the largest alpha source strength, it is still limited to jut below 2 % relative to the beams. The relative alpha ion heating rise rate is approximately half an order of magnitude per 10 MW of additional heating. On the z-axis we additionally plot the relative contribution of the alphas to the total pressure in the core (averaged within $\rho < 0.4$), computed with the alpha density and average temperature obtained through Monte Carlo particle tracking. For an alpha energy distribution slowed-down from 3.5 MeV birth energy, the average energy in the core varies between 0.9–1 MeV. One can observe that the cluster of high performing pulses recorded relative alpha pressure levels of around 3–5 %, while the T-rich achieved the highest relative contribution of $\sim$ 10 %. The core-averaged slowing-down time of the alpha particles varied between 100~640 ms, depending on plasma density and temperature, and had an average value of 330 ms for the D-T database.

Plasma heating in future fusion reactors is expected to largely affect the electron channel – both because systems aimed at electron cyclotron heating will be heavily relied on, and because dominant alpha self-heating conditions are expected to be achieved, with a predominant direct contribution to the electron power balance. In Figure 13 we show a comparison between the computed electron heating density profiles stemming from external sources (sum of NBI, RF and Ohmic heating), and alphas. The comparison is shown for individual DTE2 scenarios for selected high performing shots (a subset of discharges shown in Figure 4: baseline #99948, hybrid #99912, T-rich #99965 and EP #99802). One can observe that in contrast with the ion heating, alphas contribute to the electron heating at a level comparable with that of combined external heating sources. Both the baseline and hybrid discharges have a double-humped shape of external electron heating profile. This arises as a combination of beam power deposition dominating from $\rho > 0.4$ to the separatrix, more pronounced in the baseline case due to lower penetration at higher plasma density, and RF heating that peaks in the vicinity of the magnetic axis, within $\rho \lesssim 0.2$. The ratio of alpha over external electron heating, averaged within $\rho \leq 0.1$, is 0.20 for the baseline and 0.25 for the hybrid discharge. The EP hybrid-like discharges do not employ RF heating, therefore their external heating profile is determined by beam penetration at low electron densities, hence the core peakedness. The ratio of alpha over external electron heating in the core is 0.46. The highest absolute and relative contribution of alpha electron heating was computed for the record performing T-rich discharges. In these discharges the external heating profile has a relatively low peakedness due to the dominating beam heating over RF, with a high ratio of alpha over

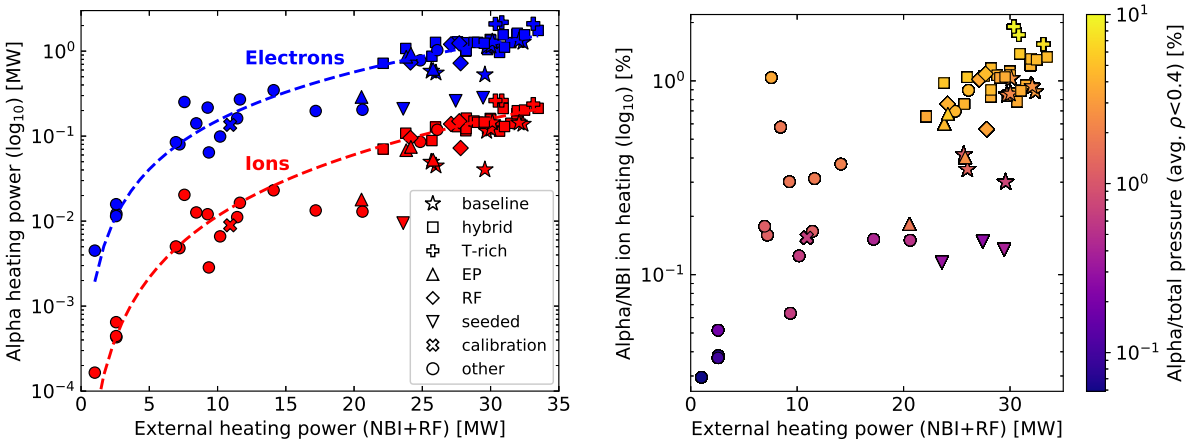

Figure 12: *Left*: alpha heating power to the electron (blue) and ion (red) channels in dependency of the external combined NBI and RF heating power for the DTE2 database. The alpha heating rise rate is fitted with a power-law function. *Right*: computed ratio between the total alpha and NBI ion heating in dependency of the external combined NBI and RF heating power. The z-axis (colorbar) denotes the ratio between the alpha and NBI ion pressure in the plasma core (averaged over $\rho < 0.4$). The graphs share the scenario type legend notation.

external electron heating in the core of 0.72. Because the alpha source term is linked to fusion reactivity all the alpha heating profiles can be observed to peaked on the magnetic axis. Although the volume-integrated contribution of the core alpha heating to the global power balance is modest, conditions in which the alpha electron heating is comparable to the sum of external electron heating sources was achieved locally in the highest performing D-T discharges.

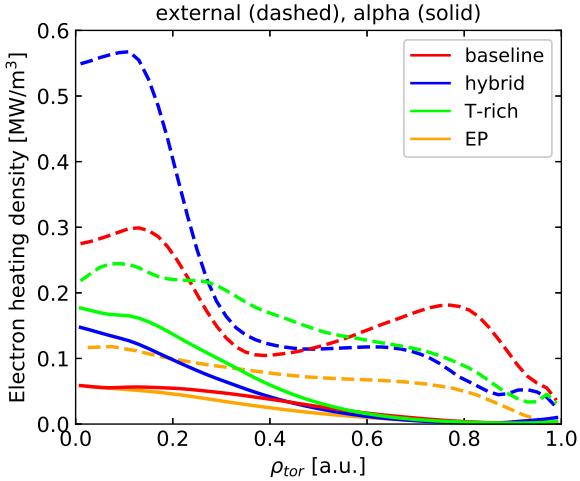

Figure 13: Comparison of the computed external (dashed – NBI+RF+Ohmic) and alpha (solid) electron heating power density profiles for a selection of best performing DTE2 discharges (baseline #99948, hybrid #99912, T-rich #99965 and EP #99802).

4. Fusion yield modelling with majority fundamental RF heating

In this section we report on the modelling workflow developed to accurately calculate the fusion yield in discharges employing the majority fundamental RF heating scheme. This posed the biggest challenge in interpretive TRANSP modelling of fusion performance for the DTE2 database, and was applicable to the record T-rich scenario. We analyse a representative T-rich pulse #99972, performed at a fuel mixture of 10:90 D-T, on-axis magnetic field of B_0 = 3.85 T, plasma current of I_p = 2.5 MA, with approximately 29 MW of deuterium NBI heating. In addition ~ 3.7 MW of ICRH power was applied at a frequency of ν_{RF} = 29 MHz, adjusted for on-axis N=1 deuterium heating [28, 32]. In this heating configuration the Maxwellian distribution of the bulk D ions is accelerated by the RF interaction and forms an energetic tail, extending to energies above several hundred keV. In addition there is a synergy effect between the RF waves and the fast beam deuteron population, via the Doppler shifted resonance, however it is not as prominent as when employing the second harmonic RF scheme. TRANSP can describe the latter effect with the quasi-linear RF kick operator [40, 41], which enables the communication of TORIC computed quantities to NUBEAM, e.g. the RF electric field components and perpendicular wave vector for each toroidal mode, and has been validated at JET [42, 18]. However TRANSP can not fully model the absorption of RF power on bulk thermal species ($< 1.5T_i$) and requires defining a dedicated fast RF minority species, with concentrations typically between 0.5 % to 5 %. While the TRANSP native FPP (Fokker-Planck Program) code solves the bounce-averaged Fokker-Planck equation to compute the fast ion distribution function $f_{RF}(E, \mu, r, t)$ – as a function of energy E, magnetic moment μ (or equivalently pitch angle ξ), minor radius r and time t – it does not have a self-collisional operator, does not communicate the RF-tail collisional term to TRANSP, assumes the background species are Maxwellian, and does not communicate the fusion output contribution to the total yield calculation. Additionally the beam-slowing down calculation is not done in consistency with the RF minority definition, with NUBEAM disregarding the RF minority density. Therefore if the RF-accelerated thermal ions are fuel particles contributing to the total yield, and the RF species density is too large to be a minority, i.e. $\gtrsim$ 5 %, an alternative modelling workflow needs to be found in order to accurately describe the heating effects.

We've solved this with the following procedure: *(i)* running a reference calculation in which the ~ 10 % bulk deuterium is considered to be a completely thermal species. This facilitates a consistent beam slowing-down calculation, providing an estimate of the beam-induced fusion contribution, including D beam–T thermal and D beam–D beam fusion, including the effects of NBI+RF synergy. *(ii)* running a repeat simulation in which the bulk deuterium is fully defined as an RF minority species, explicitly bypassing TRANSP's flag for using the same beam and RF isotope, in order to evolve it wholly as a Maxwellian with an energetic tail with FPP. The f_{RF} distribution function is averaged over a specified time interval. *(iii)* extracting the RF distribution function and using it to calculate the contribution of the deuteron Maxwellian and tail to the total fusion power. The first-step simulation results are shown in Figure 14, where we display the comparison between time-resolved measurements (red) and calculations (black) of the total neutron yield. One can observe a good match both in the absolute values and the relative shape of the yield time evolution, especially in the highest performing part of the discharge. One can observe that the performance is predominantly beam-target driven (blue), with approximately 7–8 % computed to be the thermal contribution, omitting the RF D-bulk heating. Although the beam-target calculation does not have information on the D-RF tail distribution, this will not affect its estimate due the low yield of D beam-D-RF fusion, which is true for the BB component as well. In the second-step simulation we chose to output f_{RF} in the interval of [48.8,49.0] s, denoted with the dashed grey lines in Figure 14. The RF power balance, including the D-RF minority, shows that approximately 10 % of the power is absorbed by the electrons, with the rest equally split between absorption on the D-bulk and D-beam ions, meaning that around 45 %

of RF power will be pumped into energizing the bulk Maxwellian deuterons. There is RF power absorption on fusion alphas, but is negligible and amounts to around 20 kW.

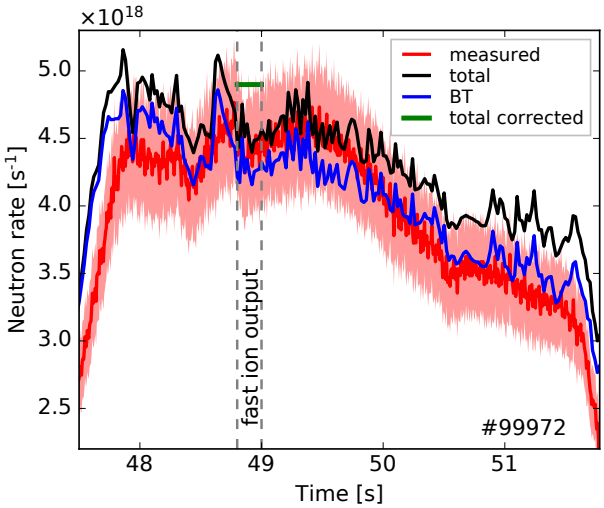

Figure 14: Comparison of the measured (red) and TRANSP computed (black) neutron rates for the T-rich D-T discharge #99972, including the beam-target component (blue) and the corrected total rate including the contribution of the RF-accelerated deuterium-bulk tail (green). The grey dashed lines denote the 0.2 s time interval over which the fast ion distribution functions were averaged. The ± 10 % experimental uncertainty is denoted with the red shaded band.

The bounce-averaged Fokker-Planck RF distribution function is defined such that the average minority density within a flux-surface averaged zone, with radius ρ and volume V, equals:

$$\langle n_{\mathrm{RF}}(\rho)\rangle = 25\ V(\rho) \int_E \int_\xi f_{\mathrm{RF}}\ \tau_{\mathrm{B}} |\xi| \sqrt{E}\ dE\ d\xi\ , \tag{5}$$

where τ_{B} is the average orbit bounce time. The normalized distribution function is integrated over the pitch angle to obtain the energy dependent function. We plot the core (ρ = 0.025) transformed f_{RF} (red) in the left-hand side panel of Figure 15, together with the D-beam (green) and fusion alpha (blue) energy distribution functions evolved by NUBEAM. One can observe that the slowed-down beam distribution has a characteristic full-half-third energy structure, with the max source energy of 100 keV, in addition to a modest synergy tail visible as an extension beyond ~ 180 keV. The low-energy part of the alpha distribution continuum can be seen, which extends up to its fusion birth energy of ~ 3.5 MeV. The calculated RF-accelerated D-bulk distribution exhibits a thermal Maxwellian shape with an exponentially decaying tail. Although the distribution extends to energies of 1 MeV, the density drops by more than two orders of magnitude compared to the Maxwellian bulk at 200 keV, and another order of magnitude by 300 keV when its concentration is lower than that of the alpha particles. f_{RF} is input into the fusion rate calculator, in which we use the beam-target fusion reactivity, plotted in the right-hand side graph of Figure 15 (blue). The reactivity shows a clear peaked shape, reaching its maximum value at 127 keV (core T_{i} = 9.8 keV). We additionally plot the energy dependency of the cumulative reaction rate density, including the D-minority and T-thermal density distributions. It can be seen that 88 % of the total fusion rate is contributed by RF-accelerated deuterons below the energy of $\langle\sigma v\rangle_{\mathrm{BT}}$ peak, while at 200 keV 98 % of the total fusion contribution is accounted for. Radially outward from the magnetic axis the RF-tail decays quickly with 90 % of the total D-bulk contribution to the fusion power reached at $\rho \sim 0.4$. The corrected total fusion power in #99972 is computed as a sum of the BT and BB components from the original run, and the TH

with an RF-tail contribution from the RF-minority run. We assess that approximately 4–5 % of the total neutron yield stems from Maxwellian fusion, while an additional 10 % is computed to results from the RF-accelerated D-bulk tail. This is in line with neutron spectrometer observations and alternative calculations reported in [32]. The corrected total neutron rate, averaged over the fast ion distribution output interval, is shown in Figure 14 with the green bar. A 10 % increase to the originally calculated TRANSP neutron yield is applied to the other two T-rich modelled discharges as well throughout the paper – we can see that it is also due to this modelling correction that the T-rich discharges are pushed into the lower part of the discharge cluster, exhibiting a fusion power overestimation due to the BT component, seen in Figure 10.

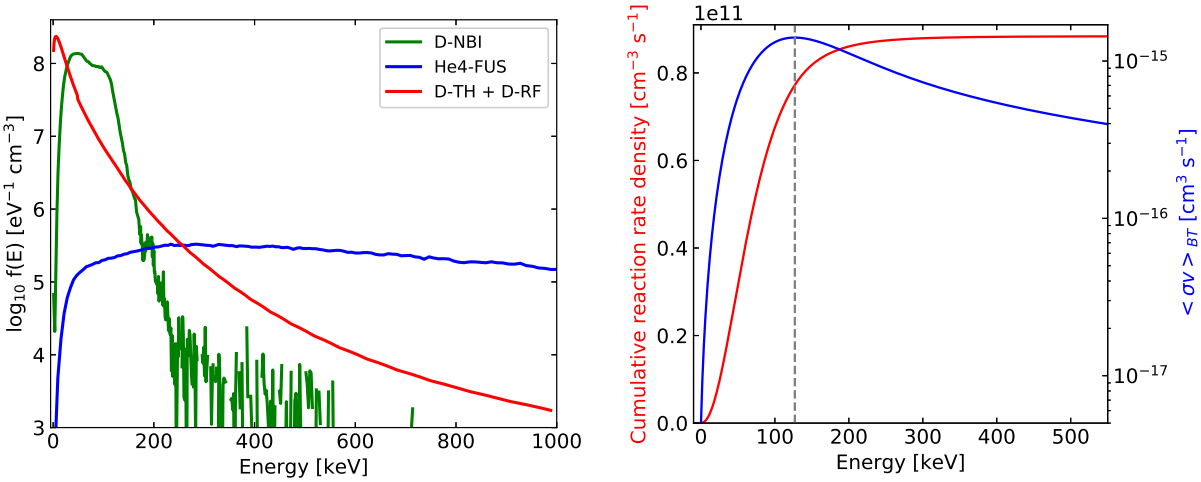

Figure 15: *Left*: calculated core ion energy distribution functions for the T-rich D-T discharge #99972, including the deuterium fast beam ion distribution (green), fusion alpha distribution (blue, extends up to ~ 3.5 MeV), and the RF-accelerated deuterium-bulk tail distribution (red). *Right*: computed core cumulative reaction rate density (red, left y-axis) and the deuterium beam → thermal T reactivity $\langle\sigma v\rangle_{\mathrm{BT}}$ (blue, right y-axis), dependent on fast ion energy. The grey line denotes the ion energy at which the maximum reactivity is reached.

5. Discussion and conclusions

New deuterium-tritium plasma experiments have been performed at JET more than 20 years after DTE1. Significant progress has been made in the understanding of tokamak physics, development of plasma modelling workflows, and improvement of JET's diagnostics systems in this time [20, 21]. In this period TRANSP has been continuously used to support JET's experimental and scientific program, predominantly through interpretive plasma analyses, inter-shot control room support, and predictive modelling. Substantial work has been done on building and verifying improved TRANSP modelling frameworks and promotion of rigorous data validation at JET [38, 48]. Additionally, significant effort was invested into validating TRANSP's synthetic diagnostics and fast ion output against experiments, e.g. the NBI and NBI+RF synergy fast ion distribution function calculations [15, 65, 79, 80], and study of fusion products and their effects on diagnostics [18, 81, 82, 83]. The compilation of a database of reliable D and D-T interpretive TRANSP runs is largely owed to a JET-wide continuos investment into the improvement of diagnostics data validation and processing, modelling framework development, and unification of modellers' assumption and techniques. In the paper we present an overview of D-T fusion performance interpretive modelling using TRANSP and its heating modules. We focus on describing the general trends observed across a wide range

of plasma operational parameters, such as the performance driving mechanisms, neutron yield component contributions, computational uncertainty dependencies, and alpha particle effects. Below we summarize the main observations of the paper, insightful for further D-T modelling and extrapolation to ITER and future fusion devices, and highlight the most pressing modelling questions that remain to be answered.

We find that interpretive simulations confirm a general power-law relationship between increasing external heating power and fusion output, which is supported by absolutely calibrated neutron yield measurements. It is shown that although the beam-induced fusion generally dominates the D-T performance over an ~ 35 MW range of P_{heat}, the thermal fusion component is strongly increasing with rising power, with the ratio of BT/TH decreasing with a weak exponential dependency. The thermal component maximization effort culminated in a set of baseline discharges that have displayed a sustained BT/TH ratio of $\gtrsim 1$. The thermal component rise correlates well with an increasing trend in total ion heating, including an increase in the gain against electron heating resulting in a favourable decoupling of ion and electron temperatures. It is shown that a majority of the highest performing discharges operated at relatively low collisionalities and high plasma rotation, both positively affecting the fusion performance through enabling good beam penetration and evolution of energetic RF-minority tails, and suppression of turbulence by increased rotational shear. The addition of RF heating is shown to have a clear positive impact on the fusion performance, both through direct induction of fusion reactions by fuel ion acceleration, or indirectly through driving an increase in T_{e} and T_{i}. The D-D extrapolation and predictive simulations in general assessed that the fusion power achieved in DTE2 would be greater by several MW, but fell within the assessed uncertainty [59, 20, 84]. In addition to the known limitations of predictive models [11], the explanation for the over-prediction of extrapolations is multi-faceted – some of the contributing factors are the lack of NBI and RF power availability, i.e. the max sustained achieved power was 30+4 MW against the assumed 34+6 MW, respectively, and several scenarios facing unexpected issues with tungsten accumulation control, expanded on in [23, 26, 28]. Note that in D-T plasmas alphas contribute up to an additional ~ 2 MW to the plasma heating, but the majority of the power is coupled to the electron channel. A fusion performance comparison between two high performing baseline and hybrid discharges shows that the latter achieved favourable electron and ion heating conditions at a rate twice as high as the baseline, yet remains dominated by beam-induced fusion reactions. The baseline discharges suffered from detrimental effects of uncontrolled n_{e} increase on performance, and only achieved a quasi-steady-state, but indicate a thermal fusion dominated discharge pathway, provided plasma control issues can be overcome. Both baseline and hybrid discharges remain interesting candidates for extrapolation to burning plasma conditions, and are relevant scenarios for ITER operations in D-T.

One of the main aims of the paper was to assess our capability of computationally reproducing the fusion performance of various D-T plasma scenarios using different external heating and fuel mixture configurations, summarized in Figure 9. Two unexpected observations are reported – that fusion power calculations for the equivalent D-ILW plasma database, of similar sample size and plasma parameters phase-space compared to DTE2, exhibit good agreement with the measurements across the whole range of P_{heat}. While an increase in deviation for beam-target driven lower-performing D shots can be seen, it is unsystematic and below the estimated uncertainty. This is in contrast to the systematic over-prediction of calculations of up to 50 % reported in previous studies, albeit dealing predominantly with discharges performed with JET's carbon wall [12, 13]. We postulate that a better agreement was achieved through a combination of favourable diagnostics and modelling improvements. These are the systematic increase in D-D neutron yield measurements of $\sim +14$ % applied to discharges performed after 2013 (improved by the use of newer standard dosimetry libraries for the neutron activation system [85]), the availability of CX measurements providing T_{i} and Ω_{t} profiles ($T_{\mathrm{i}} = T_{\mathrm{e}}$ was frequently assumed in previous work [62]), the application of the iterated pressure-constrained EFIT++ equilibrium reconstruction procedure [48] (which can significantly affect the

neutron rate due to its effect on the Shafranov shift), and overall more consistency in modelling assumptions, e.g. fitting routines, heating settings, impurity composition. Comparing measured and computed neutron rates for the DTE2 database we find a strong dependency of the discrepancy between the two and absolute neutron rate. The calculations are found to be in excellent agreement with measurements for higher performing discharges with external heating power above $\sim$ 20 MW, while low-neutron shots display an average discrepancy of around +40 %. A similar trend is found for the ratio between thermal and beam-target fusion components, where larger discrepancies are in average seen in shots with beam-driven performance. A targeted analysis in support of beam calibration has found that there are differences in the performance of individual beam lines at similar nominal power, resulting in difficulties in matching the TRANSP computed neutron yield and plasma stored energy to measurements. In addition a dependency of the D-T yield calculation over-prediction on the beam species was found, presented in detail in [78]. Similarly to our analyses, these findings indicate that the beam source term or anomalous beam ion transport might contribute to the observed discrepancy, through uncertainty in beam calibration affecting plasmas with only D or mixed D-T beams differently, and the contribution of MHD activity to anomalous diffusion. It is highly likely that these two processes contribute in a combined way in decreasing the beam ion density and altering their energy distribution function, agreeing with the observation that the BT component is over-estimated. It is important to emphasize that input D and D-T plasma parameters were not adjusted in the modelling to improve the match between the measured and calculated neutron yield, in order to assure comparability of results. A cross-code benchmark study against NUBEAM-equivalent beam slowing-down codes, such as ASCOT [86], LOCUST [73] or RABBIT [68], is proposed, predominantly aimed at validating the beam slowing-down calculation in D-T plasmas across a range of fusion performance, using identical equilibrium and kinetic profile inputs as in the presented database. A comparison between NUBEAM and ASCOT was done for D plasmas, where the beam-target fusion component was found to be larger in NUMBEAM, while the thermal and beam-beam component were consistent [63]. However due to the fact that significant differences were found in the equilibrium and profile fits used in the two codes, the observed systematic difference in the BT fusion of this study is not conclusive. Additional studies into the effect of fast ion redistribution due to MHD activity for JET D-T scenarios are proposed, specifically aimed at core localised modes using state-of-the-art workflows coupling orbit tracking and MHD codes [71, 73, 74].

An assessment of the fusion power computational uncertainty due to uncertainty in the input data shows a strong dependency on the plasma scenario due to the sensitivity to performance drive mechanisms. The combined uncorrelated uncertainty varies from approximately ± 25 % for the high-performing baseline and hybrid discharges, to $\sim$ 35 % for the calibration discharges, representative of lower performing highly BT driven plasmas. Although the mean calculated yield discrepancy for the low-power D-T discharges is relatively large at +40 %, the estimated computational uncertainty is of similar value. Appreciating the magnitude of these uncertainties – it is sobering that a fusion power calculation accurate within ± 25–35 % is the optimal obtained result with significant time invested into data validation and improvement of modelling workflows, and shows the importance of uncertainty evaluations. This implies that predictive JET D-T simulations and extrapolations to D-T plasmas in future fusion reactors can expect similar uncertainty levels on the estimated fusion power output.

Alpha particle simulations have shown that the maximum achieved total heating power was around 2 MW for the best performing pulses in DTE2, with approximately 90 % of the power flowing into the electron channel. The ratio between alpha electron and ion heating was found to be $\lesssim 10$ for the majority of the discharges, but is decreasing with a dependency of $\sim \sqrt{P_{\mathrm{heat}}}^{-1}$. The alpha ion heating power reached a maximum of 2 % with respect to that provided by beam injection, with the alpha contribution to the total pressure peaking at just below 10 %. The computed alpha distribution functions will be used as

input in further studies, investigating experimental proof of alpha heating and alpha drive of instabilities such as Alfvén eigenmodes [34, 30]. It was found that conditions in which the alpha electron heating is comparable to the sum of external electron heating sources was achieved locally in the highest performing D-T discharges, with the alpha over external electron heating ratio of ~ 0.7 in the core of T-rich shots. We additionally show that the highest performing pulses in the DTE2 campaign, part of the hybrid-like T-rich scenario, can not be modelled fully by TRANSP by default because the fundamental majority RF heating scheme was applied, aimed at D-bulk ions. Adopting a modified modelling workflow, we show that the contribution of the deuteron Maxwellian distribution with an energetic RF tail to the total fusion yield is approximately 15 %. The TRANSP FPP module, providing a quasi-consistent calculation of the effect of RF power deposition on a majority thermal ion species, is superseded by higher fidelity codes such as CQL3D [87] or FOPLA [32], which the computed distribution functions are planned to be benchmarked against.

To summarize, with a coordinated modelling effort based on rigorously validated diagnostics data, consistent modelling techniques, and improved workflows we have compiled a database of JET DTE2 TRANSP interpretive simulations. The database includes a broad spectrum of plasma scenarios with varying machine and plasma parameters. We have shown that for a majority of the database a good match between measurements and calculations of global consistency check parameters is obtained, within the estimated uncertainties. Most importantly it is shown that the calculated fusion power for the highest performing discharges of JET's D-T campaign, relevant for ITER extrapolations, is in excellent agreement with the absolutely calibrated neutron yield measurements. This provides a reliable scientific foundation and validated input for D-T predictive modelling and code development [11].

Acknowledgements

This work has been carried out within the framework of the EUROfusion Consortium, funded by the European Union via the Euratom Research and Training Programme (Grant Agreement No 101052200 — EUROfusion) and from the EPSRC [grant number EP/W006839/1]. Views and opinions expressed are however those of the author(s) only and do not necessarily reflect those of the European Union or the European Commission. Neither the European Union nor the European Commission can be held responsible for them.

References

[1] J. Breslau, M. Gorelenkova, F. Poli *et al.*, "Transp," 2018.

[2] R. J. Goldston, D. C. McCune, H. H. Towner *et al.*, "New techniques for calculating heat and particle source rates due to neutral beam injection in axisymmetric tokamaks," *Journal of Computational Physics*, vol. 43, pp. 61–78, 1981.

[3] J. P. H. E. Ongena, I. Voitsekhovitch, M. Evrard *et al.*, "Numerical transport codes," *Fusion Science and Technology*, vol. 61, pp. 180–189, 2 2012. [Online]. Available: https://www.tandfonline.com/doi/full/10.13182/FST12-A13505

[4] P. Batistoni, S. Popovichev, A. Cufar *et al.*, "14 mev calibration of jet neutron detectors - phase 1: calibration and characterization of the neutron source," *Nuclear Fusion*, vol. 58, p. 026012, 2 2018. [Online]. Available: http://stacks.iop.org/0029-5515/58/i=2/a=026012?key=crossref.62be43414208ce42d84e880519f8b59f

[5] P. Batistoni, S. Popovichev, Z. Ghani *et al.*, "14 mev calibration of jet neutron detectors - phase 2: in-vessel calibration," *Nuclear Fusion*, vol. 58, p. 106016, 10 2018. [Online]. Available: http://stacks.iop.org/0029-5515/58/i=10/a=106016?key=crossref.0f1845ba46b22a61ac624e0f7f63f80b

[6] A. Čufar, P. Batistoni, S. Conroy *et al.*, "Calculations to support in situ neutron yield calibrations at the joint european torus," *Fusion Science and Technology*, pp. 1–17, 8 2018. [Online]. Available: https://www.tandfonline.com/doi/full/10.1080/15361055.2018.1475163

[7] P. Batistoni, S. Popovichev, S. Conroy *et al.*, "Calibration of neutron detectors on the joint european torus," *Review of Scientific Instruments*, vol. 88, p. 103505, 10 2017. [Online]. Available: http://aip.scitation.org/doi/10.1063/1.4991780

[8] Ž. Štancar, M. Gorelenkova, S. Conroy *et al.*, "Multiphysics approach to plasma neutron source modelling at the jet tokamak," *Nuclear Fusion*, vol. 59, p. 096020, 9 2019. [Online]. Available: https://iopscience.iop.org/article/10.1088/1741-4326/ab2c8b

[9] R. Juarez, G. Pedroche, M. J. Loughlin *et al.*, "A full and heterogeneous model of the iter tokamak for comprehensive nuclear analyses," *Nature Energy*, vol. 6, pp. 150–157, 2 2021. [Online]. Available: http://www.nature.com/articles/s41560-020-00753-x

[10] J. Garcia, C. Challis, D. Gallart *et al.*, "Challenges in the extrapolation from dd to dt plasmas: experimental analysis and theory based predictions for jet-dt," *Plasma Physics and Controlled Fusion*, vol. 59, p. 014023, 1 2017. [Online]. Available: http://stacks.iop.org/0741-3335/59/i=1/a=014023?key=crossref.8bb345a069198fe7a669556c7dac8f5b

[11] H.-T. Kim, F. Auriemma, J. Ferreira *et al.*, "Validation of dt fusion power prediction capability against 2021 jet d-t experiments," *Submitted to Nuclear Fusion*, 2023.

[12] H. Weisen, H.-T. Kim, J. Strachan *et al.*, "The 'neutron deficit' in the jet tokamak," *Nuclear Fusion*, vol. 57, p. 076029, 7 2017.

[13] Y. F. Baranov, I. Jenkins, B. Alper *et al.*, "Anomalous and classical neutral beam fast ion diffusion on jet," *Plasma Physics and Controlled Fusion*, vol. 51, p. 044004, 4 2009.

[14] H.-T. Kim, A. Sips, C. Challis *et al.*, "1997 jet dt experiments revisited—comparative analysis of dd and dt stationary baseline discharges," *Nuclear Fusion*, vol. 60, p. 066003, 6 2020.

[15] K. Kirov, E. Belonohy, C. Challis *et al.*, "Analysis of the fusion performance, beam–target neutrons and synergistic effects of jet's high-performance pulses," *Nuclear Fusion*, vol. 61, p. 046017, 4 2021. [Online]. Available: https://iopscience.iop.org/article/10.1088/1741-4326/abdfde

[16] D. B. King, C. D. Challis, E. G. Delabie *et al.*, "Neutral beam injection on jet : Effect on neutron discrepancy and energy balance," 2018, p. P4.1067.

[17] P. Sirén, J. Varje, H. Weisen *et al.*, "Role of jetpeak database in validation of synthetic neutron camera diagnostics and ascot-afsi fast particle and fusion product calculation chain in jet," *Journal of Instrumentation*, vol. 14, pp. C11 013–C11 013, 11 2019. [Online]. Available: https://iopscience.iop.org/article/10.1088/1748-0221/14/11/C11013

[18] Ž. Štancar, Z. Ghani, J. Eriksson *et al.*, "Experimental validation of an integrated modelling approach to neutron emission studies at jet," *Nuclear Fusion*, vol. 61, p. 126030, 12 2021.

[19] L. Horton, R. Sartori, B. Balet *et al.*, "High fusion power steady state operation in jet dt plasmas," *Nuclear Fusion*, vol. 39, pp. 993–1008, 8 1999.

[20] L. Garzotti, C. Challis, R. Dumont *et al.*, "Scenario development for d–t operation at jet," *Nuclear Fusion*, vol. 59, p. 076037, 7 2019. [Online]. Available: https://iopscience.iop.org/article/10.1088/1741-4326/ab1cca

[21] J. Garcia, F. J. Casson, C. Challis *et al.*, "Integrated scenario development at jet for dt operation and iter risk mitigation," 2021, pp. EX/1–2.

[22] J. Garcia, E. de la Luna, M. Sertoli *et al.*, "New h-mode regimes with small elms and high thermal confinement in the joint european torus," *Physics of Plasmas*, vol. 29, p. 032505, 3 2022.

[23] L. Garzotti, D. Frigione, P. Lomas *et al.*, "Development of baseline scenario for high fusion performance at jet," *Submitted to Nuclear Fusion*, 2023.

[24] C. Challis, J. Garcia, M. Beurskens *et al.*, "Improved confinement in jet high β plasmas with an iter-like wall," *Nuclear Fusion*, vol. 55, p. 053031, 5 2015.

[25] C. Challis, S. Brezinsek, I. Coffey *et al.*, "Effect of fuel isotope mass on q-profile formation in jet hybrid plasmas," *Nuclear Fusion*, vol. 60, p. 086008, 8 2020.
[26] J. Hobrik, C. D. Challis, A. Kappatou *et al.*, "The jet hybrid scenario in d, t and d-t," *Submitted to Nuclear Fusion*, 2023.
[27] M. Maslov, D. King, E. Viezzer *et al.*, "Observation of enhanced ion particle transport in mixed h/d isotope plasmas on jet," *Nuclear Fusion*, vol. 58, p. 076022, 7 2018.
[28] M. Maslov, E. Lerche, C. Challis *et al.*, "T-rich scenario for the record fusion energy plasma in jet dt," *Submitted to Nuclear Fusion*, 2023.
[29] R. J. Dumont, J. Mailloux, V. Aslanyan *et al.*, "Scenario development for the observation of alpha-driven instabilities in jet dt plasmas," *Nuclear Fusion*, vol. 58, p. 082005, 8 2018.
[30] M. Fitzgerald, R. Dumont, D. Keeling *et al.*, "Stability analysis of toroidal alfven eigenmodes observed in jet deuterium-tritium internal transport barrier plasmas," *Submitted to Nuclear Fusion*, 2023.
[31] D. Gallart, M. J. Mantsinen, J. Manyer *et al.*, "Prediction of icrf minority heating schemes for jet d–t experiments," *Plasma Physics and Controlled Fusion*, vol. 64, p. 125006, 12 2022.
[32] E. Lerche, M. Maslov, P. Jacquet *et al.*, "Fundamental icrf heating of deuterium ions in jet-dte2," 2022.
[33] M. Mantsinen, P. Jacquet, E. Lerche *et al.*, "Experiments in high-performance jet plasmas in preparation of second harmonic icrf heating of tritium in iter," *Submitted to Nuclear Fusion*, 2023.
[34] P. Mantica, F. Auriemma, I. Casiraghi *et al.*, "Detection of alpha heating in jet-ilw d-t plasmas by a study of the electron temperature response to icrh modulation," 10 2023.
[35] C. Giroud, S. Brezinsek, R. A. Pitts *et al.*, "High performance iter-baseline discharges in deuterium with nitrogen and neon-seeding in the jet-ilw," 2021.
[36] A. Pankin, D. McCune, R. Andre *et al.*, "The tokamak monte carlo fast ion module nubeam in the national transport code collaboration library," *Computer Physics Communications*, vol. 159, pp. 157–184, 6 2004.
[37] M. Brambilla, "Numerical simulation of ion cyclotron waves in tokamak plasmas," *Plasma Physics and Controlled Fusion*, vol. 41, pp. 1–34, 1 1999. [Online]. Available: http://stacks.iop.org/0741-3335/41/i=1/a=002?key=crossref.6be5bf4454aa8509b29f6c6f604db3f5
[38] B. A. Grierson, X. Yuan, M. Gorelenkova *et al.*, "Orchestrating transp simulations for interpretative and predictive tokamak modeling with omfit," *Fusion Science and Technology*, vol. 74, pp. 101–115, 8 2018. [Online]. Available: https://www.tandfonline.com/doi/full/10.1080/15361055.2017.1398585
[39] O. Meneghini, S. Smith, L. Lao *et al.*, "Integrated modeling applications for tokamak experiments with omfit," *Nuclear Fusion*, vol. 55, p. 083008, 8 2015. [Online]. Available: https://iopscience.iop.org/article/10.1088/0029-5515/55/8/083008
[40] J.-M. Kwon, C. S. Chang, S.-H. Ku *et al.*, "Development of xgc-rf for global guiding-center particle simulation of minority icrh heated plasmas in a general tokamak geometry," 2006.
[41] J.-M. Kwon, D. McCune, and C. S. Chang, "Enhancement of nubeam for the simulation of fast ion and rf-wave interaction based on the quasi-linear theory," 2007.
[42] K. Kirov, Y. Baranov, I. Carvalho *et al.*, "Fast ion synergistic effects in jet high performance pulses," *Nuclear Fusion*, vol. 59, 5 2019.
[43] L. Frassinetti, M. N. A. Beurskens, R. Scannell *et al.*, "Spatial resolution of the jet thomson scattering system," *Review of Scientific Instruments*, vol. 83, p. 013506, 1 2012. [Online]. Available: http://aip.scitation.org/doi/10.1063/1.3673467
[44] S. Schmuck, J. Fessey, T. Gerbaud *et al.*, "Electron cyclotron emission measurements on jet: Michelson interferometer, new absolute calibration, and determination of electron temperature," *Review of Scientific Instruments*, vol. 83, p. 125101, 12 2012. [Online]. Available: http://aip.scitation.org/doi/10.1063/1.4768246
[45] N. C. Hawkes, E. Delabie, S. Menmuir *et al.*, "Instrumentation for the upgrade to the jet core charge-exchange spectrometers," *Review of Scientific Instruments*, vol. 89, p. 10D113, 10 2018.
[46] A. Thorman, E. Litherland-Smith, S. Menmuir *et al.*, "Visible spectroscopy of highly charged tungsten ions with the jet charge exchange diagnostic," *Physica Scripta*, vol. 96, p. 125631, 12 2021.
[47] H. Weisen, E. Delabie, J. Flanagan *et al.*, "Analysis of the inter-species power balance in jet plasmas," *Nuclear Fusion*, vol. 60, p. 036004, 3 2020. [Online]. Available: https://iopscience.iop.org/article/10.1088/1741-4326/ab6307
[48] G. Szepesi, L. Appel, E. D. la Luna *et al.*, "Advanced equilibrium reconstruction for jet with efit++," 6 2021.
[49] M. von Hellermann, P. Breger, J. Frieling *et al.*, "Analytical approximation of cross-section effects on charge exchange spectra observed in hot fusion plasmas," *Plasma Physics and Controlled Fusion*, vol. 37, pp. 71–94, 2 1995.
[50] S. Vartanian, E. Delabie, C. Klepper *et al.*, "Simultaneous h/d/t and 3he/4he absolute concentration measurements with an optical penning gauge on jet," *Fusion Engineering and Design*, vol. 170, p. 112511, 9 2021.
[51] V. Neverov, A. Kukushkin, U. Kruezi *et al.*, "Determination of isotope ratio in the divertor of jet-ilw by high-resolution h-α spectroscopy: H–d experiment and implications for d–t experiment," *Nuclear Fusion*, vol. 59, p. 046011, 4 2019.
[52] M. Sertoli, P. J. Carvalho, C. Giroud *et al.*, "Measuring the plasma composition in tokamaks with metallic plasma-facing components," *Journal of Plasma Physics*, vol. 85, p. 905850504, 10 2019.

[53] F. Casson, H. Patten, C. Bourdelle *et al.*, "Predictive multi-channel flux-driven modelling to optimise icrh tungsten control and fusion performance in jet," *Nuclear Fusion*, vol. 60, p. 066029, 6 2020.

[54] F. Köchl, A. Loarte, E. de la Luna *et al.*, "W transport and accumulation control in the termination phase of jet h-mode discharges and implications for iter," *Plasma Physics and Controlled Fusion*, vol. 60, p. 074008, 7 2018.

[55] A. Boboc, C. Gil, P. Pastor *et al.*, "Upgrade of the jet far infrared interferometer diagnostic," *Review of Scientific Instruments*, vol. 83, p. 10E341, 10 2012.

[56] B. Appelbe and J. Chittenden, "Relativistically correct dd and dt neutron spectra," *High Energy Density Physics*, vol. 11, pp. 30–35, 6 2014. [Online]. Available: http://linkinghub.elsevier.com/retrieve/pii/S1574181814000135

[57] P. Goncharov, "Spectra of neutrons from a beam-driven fusion source," *Nuclear Fusion*, vol. 55, p. 063012, 6 2015. [Online]. Available: http://stacks.iop.org/0029-5515/55/i=6/a=063012?key=crossref.ee6c784f21826e6a6a7b5a915d52964b

[58] J. Eriksson, S. Conroy, E. A. Sundén *et al.*, "Calculating fusion neutron energy spectra from arbitrary reactant distributions," *Computer Physics Communications*, vol. 199, pp. 40–46, 2 2016.

[59] E. Joffrin, S. Abduallev, M. Abhangi *et al.*, "Overview of the jet preparation for deuterium-tritium operation with the iter like-wall," *Nuclear Fusion*, vol. 59, 2019.

[60] D. V. Eester, E. Lerche, P. Huynh *et al.*, "Maximising d-t fusion power by optimising the plasma composition and beam choice in jet," *Plasma Physics and Controlled Fusion*, vol. 64, p. 055014, 5 2022.

[61] R. Budny and J. Cordey, "Core fusion power gain and alpha heating in jet, tftr, and iter," *Nuclear Fusion*, vol. 56, p. 056002, 5 2016. [Online]. Available: http://stacks.iop.org/0029-5515/56/i=5/a=056002?key=crossref.6b6441b713270e771f3ec3d90f851298

[62] H.-T. Kim, A. Sips, M. Romanelli *et al.*, "High fusion performance at high t i / t e in jet-ilw baseline plasmas with high nbi heating power and low gas puffing," *Nuclear Fusion*, vol. 58, p. 036020, 3 2018. [Online]. Available: https://iopscience.iop.org/article/10.1088/1741-4326/aaa582

[63] P. Siren, E. Tholerus, Y. Baranov *et al.*, "Comprehensive benchmark studies of ascot and transp-nubeam fast particle simulations," 7 2019, p. P4.1026.

[64] K. Kirov, C. Challis, E. D. la Luna *et al.*, "Impact of icrh heating of fast d and t ions on fusion performance in jet dte2 campaign," 2022.

[65] Y. O. Kazakov, J. Ongena, J. C. Wright *et al.*, "Physics and applications of three-ion icrf scenarios for fusion research," *Physics of Plasmas*, vol. 28, p. 020501, 2 2021. [Online]. Available: https://aip.scitation.org/doi/10.1063/5.0021818

[66] D. Gallart, M. Mantsinen, C. Challis *et al.*, "Modelling of jet hybrid plasmas with emphasis on performance of combined icrf and nbi heating," *Nuclear Fusion*, vol. 58, p. 106037, 10 2018. [Online]. Available: http://stacks.iop.org/0029-5515/58/i=10/a=106037?key=crossref.24067f8f68f87229ff6aeb62b7cfd047

[67] O. M. Jones, M. Cecconello, K. G. McClements *et al.*, "Measurements and modelling of fast-ion redistribution due to resonant mhd instabilities in mast," *Plasma Physics and Controlled Fusion*, vol. 57, p. 125009, 12 2015.

[68] M. Weiland, R. Bilato, C. Collins *et al.*, "Simulation of neutron emission in neutral beam injection heated plasmas with the real-time code rabbit," *Nuclear Fusion*, vol. 59, p. 086002, 8 2019.

[69] K. E. Thome, "Influence of energetic particle profiles on diii-d high bootstrap fraction plasmas." American Physical Society, 10 2022.

[70] G. Tardini, C. Höhbauer, R. Fischer *et al.*, "Simulation of the neutron rate in asdex upgrade h-mode discharges," *Nuclear Fusion*, vol. 53, p. 063027, 6 2013. [Online]. Available: http://stacks.iop.org/0029-5515/53/i=6/a=063027?key=crossref.e57dcf6f74da19eae4a346272951509c

[71] A. A. Teplukhina, M. Podesta, F. M. Poli *et al.*, "Fast ion transport by sawtooth instability in the presence of icrf-nbi synergy in jet plasmas," *Nuclear Fusion*, 9 2021. [Online]. Available: https://iopscience.iop.org/article/10.1088/1741-4326/ac2524

[72] H. S. Bosch and G. M. Hale, "Improved formulas for fusion cross-section and thermal reactivities," *Nuclear Fusion*, vol. 32, pp. 611–631, 1992.

[73] R. J. Akers, E. Verwichte, T. J. Martin *et al.*, "Gpgpu monte carlo calculation of gyro-phase resolved fast ion and n-state resolved neutral deuterium distributions," 7 2012, p. P5.088.

[74] M. Fitzgerald, J. Buchanan, R. Akers *et al.*, "Halo: A full-orbit model of nonlinear interaction of fast particles with eigenmodes," *Computer Physics Communications*, vol. 252, p. 106773, 2020. [Online]. Available: https://www.sciencedirect.com/science/article/pii/S0010465519301183

[75] M. Cecconello, M. Podesta, A. Jacobsen *et al.*, "Analysis of taes and fbs induced fast ions redistribution and losses in mast using a reduced fast ion transport model," 9 2019.

[76] W. Heidbrink, L. Bardoczi, C. Collins *et al.*, "The phase-space dependence of fast-ion interaction with tearing modes," *Nuclear Fusion*, vol. 58, p. 082027, 8 2018.

[77] O. N. Jarvis, E. W. Clipsham, M. A. Hone *et al.*, "Use of activation technique for the measurement of neutron yields from deuterium plasmas at the joint european torus," *Fusion Technology*, vol. 20, pp. 265–284, 11 1991. [Online]. Available: https://www.tandfonline.com/doi/full/10.13182/FST91-A29668

[78] D. B. King, R. Sharma, C. D. Challis *et al.*, "Tritium neutral beam injection on jet: Calibration and plasma measurements," *Submitted to Nuclear Fusion*, 2023.
[79] S. Mazzi, J. Garcia, D. Zarzoso *et al.*, "Enhanced performance in fusion plasmas through turbulence suppression by mega-electronvolt ions," *Nature Physics*, vol. 18, pp. 776–782, 7 2022.
[80] A. Bierwage, K. Shinohara, Y. Kazakov *et al.*, "Energy-selective confinement of fusion-born alpha particles during internal relaxations in a tokamak plasma," *Nature Communications*, vol. 13, p. 3941, 7 2022.
[81] A. Žohar, M. Nocente, B. Kos *et al.*, "Validation of realistic monte carlo plasma gamma-ray source on jet discharges," *Nuclear Fusion*, vol. 62, p. 066004, 6 2022.
[82] P. J. Bonofiglo, V. Kiptily, V. Goloborodko *et al.*, "Lost alpha faraday cup foil noise characterization during joint european torus plasma post-processing analysis," *Review of Scientific Instruments*, vol. 93, p. 093527, 9 2022.
[83] H. Järleblad, L. Stagner, M. Salewski *et al.*, "Fast-ion orbit sensitivity of neutron and gamma-ray diagnostics for one-step fusion reactions," *Nuclear Fusion*, vol. 62, p. 112005, 11 2022.
[84] J. Garcia, F. J. Casson, L. Frassinetti *et al.*, "Modelling performed for predictions of fusion power in dte2: overview and lessons learnt," *Submitted to Nuclear Fusion*, 2023.
[85] A. Trkov, P. Griffin, S. Simakov *et al.*, "Irdff-ii: A new neutron metrology library," *Nuclear Data Sheets*, vol. 163, pp. 1–108, 1 2020. [Online]. Available: https://linkinghub.elsevier.com/retrieve/pii/S0090375219300687
[86] E. Hirvijoki, O. Asunta, T. Koskela *et al.*, "Ascot: Solving the kinetic equation of minority particle species in tokamak plasmas," *Computer Physics Communications*, vol. 185, pp. 1310–1321, 4 2014.
[87] Y. V. Petrov and R. W. Harvey, "A fully-neoclassical finite-orbit-width version of the cql3d fokker–planck code," *Plasma Physics and Controlled Fusion*, vol. 58, p. 115001, 11 2016.